

SHORT RANGE ORDER AND DEVELOPMENT OF LONG RANGE ORDER  
IN NICKEL - 20 ATOMIC PERCENT MOLYBDENUM ALLOY

A THESIS

Presented to

The Faculty of the Division of Graduate

Studies and Research

by

Bhaven Chakravarti

In Partial Fulfillment

of the Requirements of the Degree

Doctor of Philosophy

in the School of Chemical Engineering

Georgia Institute of Technology

June, 1973

SHORT RANGE ORDER AND DEVELOPMENT OF LONG RANGE ORDER

IN NICKEL - 20 ATOMIC PERCENT MOLYBDENUM ALLOY

Approved by:

\_\_\_\_\_  
Dr. E. A. Starke, Jr., Chairman

\_\_\_\_\_  
Dr. Cullis J. Sparks

\_\_\_\_\_  
Dr. Bruce G. LeFevre

Date approved by Chairman: December 21, 1972

#### ACKNOWLEDGMENTS

The author is deeply indebted to his thesis advisor, Dr. Edgar A. Starke, for suggesting this research and his constant encouragement throughout the project.

A very special thanks is extended to Dr. Cullie J Sparks for his tremendous interest in the research and the continued guidance given the author. Without his help much would have remained undone.

It gives the author great pleasure to thank Dr. Ray A. Young of the Physics Department for allowing the use of the automated diffractometer for this research and Dr. Robin Williams of the Oak Ridge National Laboratory, for performing the simulation runs for the dissertation.

Finally, the author would like to thank Dr. Bruce G. LeFevre for reviewing this work. His interest and criticism is greatly appreciated.

## TABLE OF CONTENTS

	<u>Page</u>
ACKNOWLEDGMENTS . . . . .	iii
LIST OF TABLES . . . . .	v
LIST OF FIGURES . . . . .	vi
SUMMARY . . . . .	vii
Chapter	
I. INTRODUCTION . . . . .	1
II. THEORY . . . . .	5
III. EXPERIMENTAL METHODS . . . . .	15
IV. RESULTS AND DISCUSSION . . . . .	20
V. CONCLUSIONS AND RECOMMENDATIONS . . . . .	59
APPENDIX A	
Diffuse Intensity Maps and Tables . . . . .	61
APPENDIX B	
Computer Programs . . . . .	79
BIBLIOGRAPHY . . . . .	95
VITA . . . . .	97

## LIST OF TABLES

Table		Page
1.	Physical Constants . . . . .	17
2.	Measured Three-Dimensional Short-Range Order Coefficients of $\text{Ni}_4\text{Mo}$ for as-quenched, 5 and 10 Minutes Ordered at $650^\circ\text{C}$ . . . . .	44
3.	Comparison of Alphas Measured and Those Obtained from the Computer Model . . . . .	46
4.	Joint Population of Molybdenum Atoms for (110-200) Shells for a Random $\text{Ni}_4\text{Mo}$ Alloy . . . . .	47
5.	Joint Population of Molybdenum Atoms for (110-200) Shells for As-Quenched $\text{Ni}_4\text{Mo}$ Alloy . . . . .	48
6.	Three-dimensional First Order Size Effect Coefficients for the As-Quenched Alloy . . . . .	55
7.	Three-dimensional First Order Size Effect Coefficients for the Sample Ordered for 5 Minutes at $650^\circ\text{C}$ . . . . .	56
8.	Three-dimensional First Order Size Effect Coefficients for the Sample Ordered for 10 Minutes at $650^\circ\text{C}$ . . . . .	57

## LIST OF FIGURES

Figure		Page
1.	The Regions of Reciprocal Space for Making Volume Measurements of Diffuse Scattering for Cubic Systems . . . . .	12
2a-f.	Diffuse Intensity Distribution on ( $h_1, h_2, h_3 = 0.00$ to $0.25$ ) Planes of Reciprocal Space for As-Quenched $Ni_4Mo$ . . . . .	21-26
3a-f.	Diffuse Intensity Distribution on ( $h_1, h_2, h_3 = 0.00$ to $0.25$ ) Planes of Reciprocal Space for 5 Minutes Ordered Sample . . . . .	27-32
4.	Plot of Corrected Intensity Along $[420]$ Directions on $(100)$ Plane . . . . .	34
5.	3D Map of Measured Diffuse Intensity on the ( $h_1, h_2, h_3 = 0.00$ ) Plane of $Ni_4Mo$ Ordered for 5 Minutes at $650^\circ C$ . . . . .	35
6.	A Schematic of the Intensity Distribution on the $(200)$ Plane of $Ni_4Mo$ as Shown by Reference 5 . . . . .	36
7a-f.	Distribution of the Separated Short-Range Order Intensity in Reciprocal Space . . . . .	38-43
8.	Atomic Arrangements of Computer Generated Model for As-Quenched Alloy . . . . .	50
9.	Atomic Arrangements of Computer Generated Model for Alloy Aged for 5 Minutes at $650^\circ C$ . . . . .	51
10.	Atomic Arrangements of Computer Generated Model for As-Quenched $Ni_4Mo$ Showing Rodlike Morphology . . . . .	53
11.	Atomic Arrangement of Computer Generated Model of Alloy Aged 5 Minutes at $650^\circ C$ . The Rodlike Morphology can be seen to be growing. . . . .	54

## SUMMARY

The short-range ordered structure present in as-quenched  $\text{Ni}_4\text{Mo}$  and the initial development of the long-range-ordered structure has been studied using single crystal x-ray diffuse scattering techniques. Measurements of the diffuse x-ray intensities were made in a minimum volume in reciprocal space for the fcc alloy, so that quantitative determination of local-order parameters could be made. The "size effect" coefficients for the first and second order displacement effects were separated from those due to local order and their values were determined. The local-order parameters were used for a computer simulation of an average atomic configuration.

The atomic model developed for the as-quenched structure which "fits" the first five experimental SRO coefficients shows that the local atomic arrangements consist of clusters of molybdenum atoms in the {100} planes. The atoms within the clusters satisfy the long-range-ordered structure of  $\text{Ni}_4\text{Mo}$  since there are no Mo-Mo pairs as first neighbors, only one as second neighbors and six or more as third neighbors. The rodlike morphology of the molybdenum clusters grows on ordering for 5 minutes at  $650^\circ\text{C}$ . This result corroborates the rodlike morphology present in dilute Ni-W alloys and explains the [100] streaking observed in the diffraction studies.

## CHAPTER I

## INTRODUCTION

The order-disorder transformation in nickel-20 atomic percent molybdenum,  $\text{Ni}_4\text{Mo}$ , alloy has been the subject of considerable study for the past ten years (1-10). The transformation occurs at  $868^\circ\text{C}$  and undergoes a crystal structure change from the disordered face-centered cubic (fcc) to the ordered body-centered tetragonal (bct) phase (10). Both electron microscopy and x-ray diffraction have been used to characterize the kinetics and mechanism of the transformation (1-10).

Spruiell (3) performed a two-dimensional x-ray diffuse scattering measurement on the as-quenched alloy and constructed a model for the short-range order (SRO) structure present. He concluded that the SRO structure consisted of small regions in which the atomic arrangements are quite similar to the long-range ordered (LRO)  $\text{Ni}_4\text{Mo}$  structure. This description has lead to the "microdomain theory" for ordering in  $\text{Ni}_4\text{Mo}$  (8,9). The development of LRO is assumed to proceed by the growth of tiny ordered domains which are embedded in a random matrix. Ruedl et al (8) have claimed to observe such domains in dark-field electron micrographs. Consequently, the SRO diffuse peaks are considered as broad superlattice reflections and should occur at the same positions in reciprocal space as the superlattice peaks. However, they do not.

On the other hand, Clapp and Moss (11) from theoretical considerations of interaction potentials reproduced the diffuse intensity



distribution obtained by Spruiell et al (3). They discount the microdomain concept for ordering in  $\text{Ni}_4\text{Mo}$  since their statistical thermodynamic model of SRO could describe the local order in the as-quenched alloy. Field-ion studies of LeFevre et al (4,7) have also failed to substantiate the presence of microdomains in  $\text{Ni}_4\text{Mo}$ .

Okamoto (5) has suggested a modification of the domain concept using the layered structure of LRO  $\text{Ni}_4\text{Mo}$ . He shows that as-quenched  $\text{Ni}_4\text{Mo}$  contains some form of ordered domains in all the six orientation variants of the  $\text{Ni}_4\text{Mo}$  structure, and suggests that the diffuse  $1\frac{1}{2}0$  peaks can be attributed to non-conservative antiphase boundaries within these microdomains. Okamoto (5) questions such a description for the disordered alloy since it would require the presence of superlattice reflections above the critical temperature,  $T_c$ ! The problem lies in the fact that no complete description exists for the disordered alloy.

Warren (14) has shown that the pair probability function  $P_{lmn}^{BA}$  can be obtained directly from the coefficients of the Fourier expansion of the diffuse x-ray intensity corresponding to local order in a binary alloy. If the intensity is known within its repeat volume, the pair probabilities are obtained uniquely by inverting the equation:

$$I_{\text{SRO}} = N X_A X_B (f_A - f_B)^2 \sum_l \sum_m \sum_n \left(1 - \frac{P_{lmn}^{BA}}{X_B}\right) \exp(i\vec{k} \cdot \vec{R}_{lmn}) \quad [1]$$

where  $X_A$  and  $X_B$  are the atomic fractions of the species A and B having  $f_A$  and  $f_B$  as their respective atomic scattering factors.  $\vec{k}$  is the reciprocal lattice vector,  $\frac{\vec{S} - \vec{S}_0}{\lambda} = h_1 \vec{b}_1 + h_2 \vec{b}_2 + h_3 \vec{b}_3$  where  $\vec{b}_1 = 2/a_1$ .  $\vec{R}_{lmn}$  is the interatomic vector for the position defined by

coordinates  $l, m, n$ , and  $N$  is the total number of atoms irradiated by the beam.  $(1 - P_{lmn}^{BA} / X_B)$  is the Warren short-range order parameter,  $\alpha_{lmn}$ , where  $P_{lmn}^{BA}$  is the probability of finding a B atom in the  $lmn$  shell after having found the A atom at the origin. Thus if we measure the diffuse x-ray scattering corresponding to local order we can obtain an average atomic configuration for the structure under investigation.

The diffuse x-ray scattering measured contains contributions not only due to local order but also due to other factors. Most of these, such as Compton scattering, air scattering and fluorescence of the alloy sample, can be corrected for by either theoretical or experimental methods. Contributions in the diffuse intensity due to first and second order thermal diffuse scattering (TDS), size-effect modulations, the Huang peak, have previously been separated by a theoretical analysis which introduced unavoidable assumptions regarding the nature of these effects. Recently, Borie and Sparks (16) proposed a theoretical method which allows one to correct for the above mentioned effects using the experimentally measured intensities. This allows the recovery of  $I_{SRO}$  unaffected by the size-effect contributions. Then, with the use of equation 1, the required pair probabilities for the determination of the average configuration of the as-quenched alloy can be obtained. A knowledge of the pair probability function  $P_{lmn}^{BA}$  allows the simulation of an atomic configuration within a crystal lattice that satisfies the given pair probabilities. Such a method was first used by Gehlen and Cohen (12) and later by Williams (13).

Spruiell's et. al (3) data was two-dimensional and did not allow a unique determination of the pair probabilities. Therefore, their data

cannot be used for the simulation of the atomic configuration of the as-quenched alloy. Because of these uncertainties, a more exact description of the as-quenched alloy derived from three-dimensional data was felt worthwhile. The primary goal of this research was to use x-ray diffuse scattering and the 3D method of Borie and Sparks (15-17) to quantitatively study the state of local order, and follow the initial development of LRO in  $\text{Ni}_4\text{Mo}$ . The pair probabilities determined would then be applied to structure simulation so that a better understanding of short-range order and development of the long-range order might be possible.

## CHAPTER II

## THEORY

The theory pertaining to the x-ray diffuse scattering from binary has been very extensively reviewed (15) and reproduced in various dissertations (3,18-20), and will not be repeated here. The purpose of this section will be to summarize the theory and to introduce the necessary equations for the three dimensional separation method.

According to the kinematic theory of x-ray diffraction, the total coherent intensity in electron units is given by the formula

$$I_{eu} = \sum_p \sum_q f_p f_q \exp \{i\vec{K} \cdot (\vec{R}_o - \vec{R}_q)\} \quad [2]$$

where  $f_p$  and  $f_q$  are the atomic scattering factors for the atoms located at sites  $p$  and  $q$  which are separated by the interatomic lattice vector  $\vec{R}_p - \vec{R}_q$ . In a real binary substitutional solid solution, the atom positions in the crystal lattice are often displaced from their nodal positions due to atomic size differences and thermal vibrations. If we include these static and dynamic displacements, the lattice vector becomes

$$(\vec{R}_p - \vec{R}_q) + (\vec{\delta}_p - \vec{\delta}_q)$$

where  $\vec{\delta}_p$  and  $\vec{\delta}_q$  represent the displacements from the nodal positions. Substituting this in equation 2 we obtain

$$I_{eu} = \sum_p \sum_q f_p f_q \exp \{i\vec{k} \cdot (\vec{R}_p - \vec{R}_q)\} \exp \{i\vec{k} \cdot (\vec{\delta}_p - \vec{\delta}_q)\} \quad [3]$$

By expanding the second exponential to include second order terms, and introducing the concept of order through the Warren short-range order coefficient,  $\alpha_{lmn}$ , Borie and Sparks (16) have shown that the total coherently scattered intensity can be written as

$$\begin{aligned} I_{eu} = & \sum_p \sum_q (X_A f_A + X_B f_B)^2 \exp \langle i\vec{k} \cdot \vec{R}_{pq} \rangle \\ & + \sum_p \sum_q X_A X_B (f_A - f_B)^2 \alpha_{pq} \exp \langle i\vec{k} \cdot \vec{R}_{pq} \rangle \\ & + \sum_p \sum_q \{ (X_A^2 + X_A X_B \alpha_{pq}) f_A^2 \langle i\vec{k} \cdot (\vec{\delta}_p^A - \vec{\delta}_q^A) \rangle \\ & \quad + 2X_A X_B f_A f_B (1 - \alpha_{pq}) \langle i\vec{k} \cdot (\vec{\delta}_p^A - \vec{\delta}_q^B) \rangle \\ & \quad + (X_B^2 + X_A X_B \alpha_{pq}) f_B^2 \langle i\vec{k} \cdot (\vec{\delta}_p^B - \vec{\delta}_q^B) \rangle \} \exp \langle i\vec{k} \cdot \vec{R}_{pq} \rangle \\ & - \frac{1}{2} \sum_p \sum_q \{ (X_A^2 + X_A X_B \alpha_{pq}) f_A^2 \langle [\vec{k} \cdot (\vec{\delta}_p^A - \vec{\delta}_q^A)]^2 \rangle \\ & \quad + 2X_A X_B f_A f_B (1 - \alpha_{pq}) \langle [\vec{k} \cdot (\vec{\delta}_p^A - \vec{\delta}_q^B)]^2 \rangle \\ & \quad + (X_B^2 + X_A X_B \alpha_{pq}) f_B^2 \langle [\vec{k} \cdot (\vec{\delta}_p^B - \vec{\delta}_q^B)]^2 \rangle \} \exp \langle i\vec{k} \cdot \vec{R}_{pq} \rangle \end{aligned}$$

where  $\alpha_{pq}$  is the Warren short-range order parameter.

The first sum of equation 4 is the intensity of the fundamental reflections unaffected by local order or static and dynamic displacements. The second sum is the Laue monotonic intensity modulated by the order parameter,  $\alpha_{pq}$ . The third sum is the "size effect" or static displacement modulated intensity since  $i\vec{K}(\vec{\delta}_p - \vec{\delta}_q) = 0$  for thermal motion using a harmonic oscillator model. Effects due to both thermal and static distortion are contained in the fourth sum. These include the first order temperature diffuse scattering and the Huang intensity. When this fourth sum is examined for convergence, it is found that a negative delta function is produced which peaks at the fundamental reflection positions. Physically this means that the mean square atomic displacements, which are acting cooperatively over long distances in the crystal, reduce the intensity of the fundamental reflections. The intensity lost by the fundamental reflections is redistributed as Huang and TDS. Thus if the limiting value of the mean square displacement is added to the first sum and subtracted from the fourth sum (when expressed in terms of a set of correlated displacement parameters), the intensity expression is immediately separable into two parts. One part represents the sharp crystalline reflections which are reduced in intensity for the reason just cited, and the other describes the diffuse intensity.

These are:

$$I_{\text{Fund}} = \sum_p \sum_q (X_A f_A e^{-M_A} + X_B f_B e^{-M_B})^2 \exp\langle i\vec{K} \cdot \vec{R}_{pq} \rangle \quad [5]$$

which is just like the fundamental reflection reduced in intensity by

the factor  $e^{-M}$  for each atom; and

$$\begin{aligned}
 I_{\text{Diffuse}} = & \sum_p \sum_q X_A X_B (f_A - f_B)^2 \alpha_{pq} \exp \langle i \vec{K} \cdot \vec{R}_{pq} \rangle \\
 & + \sum_p \sum_q X_A X_B (f_A - f_B) \left( \frac{X_A}{X_B} + \alpha_{pq} \right) f_A \langle i \vec{K} (\vec{\delta}_p^A - \vec{\delta}_q^A) \rangle \\
 & - \left( \frac{X_B}{X_A} + \alpha_{pq} \right) f_B \langle i \vec{K} (\vec{\delta}_p^B - \vec{\delta}_q^B) \rangle \exp \langle i \vec{K} \cdot \vec{R}_{pq} \rangle \\
 & - \sum_p \sum_q \{ X_A X_B (f_A - f_B) [(X_A + X_B \alpha_{pq}) f_A \langle (\vec{K} \cdot \vec{\delta}_p^A)^2 \rangle_A \\
 & - X_A (1 - \alpha_{pq}) f_A \langle (\vec{K} \cdot \vec{\delta}_p^A)^2 \rangle_q + X_B (1 - \alpha_{pq}) f_B \langle (\vec{K} \cdot \vec{\delta}_p^B)^2 \rangle_q \\
 & - (X_B + X_A \alpha_{pq}) f_B \langle (\vec{K} \cdot \vec{\delta}_p^B)^2 \rangle_q] \\
 & - X_A f_A^2 (X_A + X_B \alpha_{pq}) \langle (\vec{K} \cdot \vec{\delta}_p^A) (\vec{K} \cdot \vec{\delta}_q^A) \rangle \\
 & - 2 X_A X_B (1 - \alpha_{pq}) f_A f_B \langle (\vec{K} \cdot \vec{\delta}_p^A) (\vec{K} \cdot \vec{\delta}_q^B) \rangle \\
 & - X_B f_B^2 (X_B + X_A \alpha_{pq}) \langle (\vec{K} \cdot \vec{\delta}_p^B) (\vec{K} \cdot \vec{\delta}_q^B) \rangle \} \exp \langle i \vec{K} \cdot \vec{R}_{pq} \rangle
 \end{aligned}$$

[6]

The above equations are completely general to the second order approximation for the displacement effects and may be used for any crystal structure containing two atomic species. For face-centered and body-centered cubic substitutional solid solutions,  $i \vec{K} \cdot \vec{R}_{pq} = 2\pi i(h_1 l + h_2 m + h_3 n)$  since  $\vec{K} = 2\pi(h_1 \vec{b}_1 + h_2 \vec{b}_2 + h_3 \vec{b}_3)$  and  $\vec{R}_{pq} =$

$la_1/2 + ma_2/2 + na_3/2$ .  $h_1$ ,  $h_2$  and  $h_3$  are continuous variables in reciprocal space. Equation 6 reduces to (17)

$$\begin{aligned}
 I_{\text{Diffuse}} = & NX_A X_B (f_A - f_B)^2 \sum_l \sum_m \sum_n \alpha_{lmn} (\cos 2\pi h_1 l) (\cos 2\pi h_2 m) (\cos 2\pi h_3 n) \\
 & - NX_A X_B (f_A - f_B)^2 \sum_l \sum_m \sum_n \{ h_1 \gamma_{lmn}^1 (\sin 2\pi h_1 l) (\cos 2\pi h_2 m) (\cos 2\pi h_3 n) \\
 & + h_2 \gamma_{lmn}^m (\cos 2\pi h_1 l) (\sin 2\pi h_2 m) \\
 & (\cos 2\pi h_3 n) \\
 & + h_3 \gamma_{lmn}^n (\cos 2\pi h_1 l) (\cos 2\pi h_2 m) \\
 & (\sin 2\pi h_3 n) \} \\
 & - 4\pi^2 N \sum_l \sum_m \sum_n (h_1^2 \langle \partial^2 \rangle_{lmn}^1 + h_2^2 \langle \partial^2 \rangle_{lmn}^m + h_3^2 \langle \partial^2 \rangle_{lmn}^n) \\
 & \times \{ (\cos 2\pi h_1 l) (\cos 2\pi h_2 m) (\cos 2\pi h_3 n) \\
 & + 8\pi^2 N \sum_l \sum_m \sum_n \{ h_1 h_2 \langle \partial^2 \rangle_{lmn}^{1m} (\sin 2\pi h_1 l) (\sin 2\pi h_2 m) (\cos 2\pi h_3 n) \\
 & + h_1 h_3 \langle \partial^2 \rangle_{lmn}^{1n} (\sin 2\pi h_1 l) (\cos 2\pi h_2 m) (\sin 2\pi h_3 n) \\
 & + h_2 h_3 \langle \partial^2 \rangle_{lmn}^{mn} (\cos 2\pi h_1 l) (\sin 2\pi h_2 m) (\sin 2\pi h_3 n) \}
 \end{aligned}$$



with all sums extending from  $-N$  to  $N$ .

Here

$$\gamma^1 = \frac{2\pi}{f_A - f_B} \left[ \left( \frac{X_A}{X_B} + \alpha_{lmn} \right) f_A \langle X^{AA} \rangle_{lmn} - \left( \frac{X_B}{X_A} + \alpha_{lmn} \right) f_B \langle X^{BB} \rangle_{lmn} \right] \quad [7.1]$$

$$\begin{aligned} \langle \delta^2 \rangle_{lmn}^1 &= X_A X_B (f_A - f_B) \left[ (X_A + X_B \alpha_{lmn}) f_A \langle (X^A)^2 \rangle_{lmn}^A - X_A (1 - \alpha_{lmn}) f_A \langle (X^A)^2 \rangle_{lmn}^B \right. \\ &\quad \left. + X_B (1 - \alpha_{lmn}) f_B \langle (X^B)^2 \rangle_{lmn}^A - (X_B + X_A \alpha_{lmn}) f_B \langle (X^B)^2 \rangle_{lmn}^B \right] \\ &\quad - X_A (X_A + X_B \alpha_{lmn}) f_A^2 \langle X^A X^A \rangle_{lmn} - 2 X_A X_B (1 - \alpha_{lmn}) f_A f_B \langle X^A X^B \rangle \\ &\quad - X_B (X_B + X_A \alpha_{lmn}) f_B^2 \langle X^B X^B \rangle \quad [7.2] \end{aligned}$$

$$\begin{aligned} \langle \delta^2 \rangle_{lmn}^{1m} &= X_A X_B (f_A - f_B) \left[ (X_A + X_B \alpha_{lmn}) f_A \langle (XY)^A \rangle_{lmn}^A + X_B (1 - \alpha_{lmn}) f_A \langle (XY)^A \rangle_{lmn}^B \right. \\ &\quad \left. - X_A (1 - \alpha_{lmn}) f_B \langle (XY)^B \rangle_{lmn}^A - (X_B + X_A \alpha_{lmn}) f_B \langle (XY)^B \rangle_{lmn}^B \right] \\ &\quad - X_A (X_A + X_B \alpha_{lmn}) f_A^2 \langle X^A Y^A \rangle - 2 X_A X_B (1 - \alpha_{lmn}) f_A f_B \langle X^A Y^B \rangle \\ &\quad - X_B (X_B + X_A \alpha_{lmn}) f_B^2 \langle X^B Y^B \rangle \quad [7.3] \end{aligned}$$

The equation is based on the following assumptions:

- (i) The magnitude of the displacements is sufficiently small to be adequately described by first and second order terms;
- (ii) The ratio of the atomic scattering factors,  $f_A/f_B$  is constant over the reciprocal space volume in which the measurements are made.

The coefficients of each sum may be recovered since each has a different dependence on  $h_1$ ,  $h_2$  and  $h_3$ .

Following Borie and Sparks (16) we define our operator  $\Delta$  as,

$$T1H2 = \Delta(h_2-1)I(h_1, h_2, h_3) = I(h_1, h_2, h_3) - I(h_1, h_2-1, h_3)$$

$$\begin{aligned} &= -NX \sum_A \sum_B (f_A f_B)^2 \sum_l \sum_m \sum_n \gamma_{lmn}^m (\cos 2\pi h_1 l) (\sin 2\pi h_2 m) (\cos 2\pi h_3 n) \\ &+ 4\pi^2 N \sum_l \sum_m \sum_n (1-2h_2) \langle \partial^2 \rangle_{lmn}^m (\cos 2\pi h_1 l) (\cos 2\pi h_2 m) (\cos 2\pi h_3 n) \\ &+ 8\pi^2 N \sum_l \sum_m \sum_n \{h_1 \langle \partial^2 \rangle_{lmn}^{lm} (\sin 2\pi h_1 l) (\sin 2\pi h_2 m) (\cos 2\pi h_3 n) \\ &\quad + h_3 \langle \partial^2 \rangle_{lmn}^{mn} (\cos 2\pi h_1 l) (\sin 2\pi h_2 m) (\sin 2\pi h_3 n)\} \end{aligned} \quad [8]$$

With reference to Figure 1a, the difference in intensity on subtracting point B from A is the  $\Delta$  operation. If this operation is performed over the whole volume, the function represented by Equation 8 will be known in the volume shown in Figure 1b. The difference operator, T2H2, is obtained by performing the same operation on the volume shown in Figure 1b.

$$T2H2 = \Delta^2(h_2-1)I(h_1, h_2, h_3) = \Delta(h_2-1)I(h_1, h_2, h_3) - \Delta(h_2-1)I(h_1, h_2-1, h_3)$$

$$= -8\pi^2 N \sum_l \sum_m \sum_n \langle \partial^2 \rangle_{lmn}^m (\cos 2\pi h_1 l) (\cos 2\pi h_2 m) (\cos 2\pi h_3 n) \quad [9]$$



Having recovered the function given in Equation 9, the other two functions containing  $\langle \partial^2 \rangle_{lmn}^1$  and  $\langle \partial^2 \rangle_{lmn}^n$  can be generated by interchanging the indices  $h_1$  with  $h_2$  and  $h_2$  with  $h_3$ , respectively, since the alloy is statistically cubic. Sparks (17) has shown that the function represented by equation 9 is defined everywhere in reciprocal space if it is known in the volumes shown in Figures 1c or 1d for the fcc or bcc structures, respectively. A plane containing the symmetry axis 'fg' cuts the volume in half leaving the choice of the repeat volume rather flexible. The size and shape of this repeat volume is the same as that for the function  $\gamma_{lmn}^m$ . Figure 1e and 1f shows the volume of diffuse intensity data necessary to obtain the minimum repeat volume for the function  $\langle \partial^2 \rangle_{lmn}^m$  for face-centered and body-centered cubic structures respectively.

By performing the operation  $\Delta(2-h_1)$  on equation 8 we have the result that

$$\begin{aligned} T1H1 &= \Delta(2-h_1)\Delta(h_2-1)I(h_1, h_2, h_3) = \Delta(h_2-1)I(h_1, h_2, h_3) - \Delta(h_2-1)I(2-h_1, h_2, h_3) \\ &= 16\pi^2 N \sum_l \sum_m \sum_n \langle \partial^2 \rangle_{lmn}^1 (\sin 2\pi h_1 l) (\sin 2\pi h_2 m) (\cos 2\pi h_3 n) \quad [10] \end{aligned}$$

The volume of diffuse intensity data needed to do this separation is shown in Figure 1g where the intensity (D-C) is subtracted from the intensity (A-B) for the fcc structure and Figure 1h for the bcc structure. The other two functions containing  $\langle \partial^2 \rangle_{lmn}^{1n}$  and  $\langle \partial^2 \rangle_{lmn}^{mn}$  can be generated from the recovered function of equation 10 by interchanging  $h_3$  for  $h_2$  and  $h_3$  for  $h_1$ , respectively.

The function  $\sum_l \sum_m \sum_n \gamma_{lmn}^m (\cos 2\pi h_1 l) (\sin 2\pi h_2 m) (\cos 2\pi h_3 n)$  can now

be recovered from the intensity distribution represented by equation 8, since the value of the latter two sums is known. Likewise it is straightforward to recover the remaining function  $\sum_l \sum_m \sum_n \alpha_{lmn} (\cos 2\pi h_1 l) (\cos 2\pi h_2 m) (\cos 2\pi h_3 n)$  from equation 7 since all the other terms are known.

One of the many possible volumes in reciprocal space in which the measured intensity distribution is sufficient to allow a complete separation of the four different kinds of terms given in equation 7 is made by combining the volumes of Figure 1e and 1g or Figure 1f and 1h for the fcc and bcc cases, respectively. These volumes are shown in Figure 1i and 1j for fcc and bcc respectively.

The three dimensional analysis of Borie and Sparks (16) described in this Chapter allows a determination of the coefficients  $\alpha_{lmn}$ ,  $\gamma_{lmn}^m$ ,  $\langle \partial^2 \rangle_{lmn}^m$ ,  $\langle \partial^2 \rangle_{lmn}^{lm}$ . With these coefficients, a probable atomic configuration of the alloy can be computer simulated using the method of Williams (13).

## CHAPTER III

## EXPERIMENTAL METHODS

The method just described requires that the total diffuse scattered intensity be measured over the volume of reciprocal space shown in Figure 1i, using a single crystal sample. The  $\text{Ni}_4\text{Mo}$  single crystal was supplied by Dr. J. E. Spruiell of the University of Tennessee. The single crystal was oriented to have the (210) planes parallel to the surface; an orientation which allows maximum accessibility to the region of principal interest in reciprocal space.

The measurements of the total diffuse scattered intensity were made utilizing a four-circle goniometer described elsewhere (23). This completely automated unit was driven by a Datex unit which reads instructions from a paper tape. The diffractometer was aligned and a (111) oriented silicon single crystal was used to determine the true zero in  $2\theta$ . The horizontal and vertical divergences of the slit system was 1.5 and 3.0 degrees respectively. The incident beam from the copper tube (34KV, 14ma) was monochromated using a doubly-bent pyrolytic graphite monochromator.\* The half-wavelength as well as the higher order harmonics that pass the monochromator were removed using balanced filters in the incident beam. This procedure removes the occurrence of fluorescence from the sample which would otherwise add to the total measured diffuse scattering. The single crystal was carefully aligned

---

\* Very kindly loaned to us by Dr. C. J. Sparks of Oak Ridge National Laboratory.

and the true zero's of  $2\theta$ ,  $\phi$ ,  $\chi$  found and set. The sample was placed in a helium gas chamber to reduce air scattering. A scatter slit placed between the sample chamber and the detector prohibited the radiation scattered by the chamber walls from entering the detector.

The measurements of the total diffuse scattering intensity were made over 6 planes along the  $h_3$  direction, and represented a set of 1576 points on a square grid in reciprocal space spread uniformly over the volume of Figure 1i at intervals of  $\Delta h_1 = 0.05$  in the reciprocal lattice. Based on the initial orientation of the single crystal, the  $\chi$ ,  $\phi$  and  $2\theta$  setting for each of these points was computed by the program DIFVOL (listed in the appendix) and these settings converted to Datex instructions and punched onto a paper tape. A check point was programmed in the tape, so that after every 50 data points, this check point would be read in order to monitor any power fluctuations of the primary beam. Corrections due to the fluctuations were made by normalizing the data with respect to the check point.

The conversion of the measured diffuse scattered intensity to absolute electron scattering units was made by measuring the amorphous scattering from polystyrene ( $C_8H_8$ ) at 100 degrees  $2\theta$  and using the physical constants in Table 1. This intensity was then corrected for polarization factor, resonance x-rays\* (25) and Compton scattering and finally divided by the Laue Monotonic intensity. The atomic scattering factors used were corrected for dispersion effects. The Compton scattered intensity was computed from values of the incoherent scattering

---

\* The value of the nickel resonance was measured by Dr. C. J. Sparks of Oak Ridge National Laboratory.

Table 1. Physical Constants

$$X_{\text{Mo}} = X_{\text{A}} = 0.20$$

$$a_{\text{O}}(\text{Ni}_4\text{Mo}) = 3.608 \text{ \AA}$$

$$\lambda_{\text{CuK}\alpha} = 1.54178 \text{ \AA}$$

$$2\theta_{\text{monochromator}} = 26.62^\circ$$

$$2\theta_{\text{polystyrene}} = 100.00^\circ$$

$$\frac{\mu}{\rho} \text{ for Ni}_4\text{Mo} = 75.5 \text{ cm}^2/\text{gm}$$

$$\frac{\mu}{\rho} \text{ for polystyrene} = 4.036 \text{ cm}^2/\text{gm}$$

$$\frac{I_{\text{eu}}}{N} = 65.00$$



function given by Compton and Allison (24). The various corrections were performed by the program INTCOR, written for such work. The resulting intensity represented the diffuse intensity modulated by local order, size effects, and thermal diffuse scattering.

The separation, as described in Chapter II, of the various components of the diffuse intensity is performed by program SEPRIT, written to do the three dimensional separation for the quadratic approximation case. The output of this program gives us the various intensity components in their respective repeat volumes for recovering the coefficients,  $\alpha_{lmn}$ ,  $\gamma_{lmn}^m$ ,  $\langle \delta^2 \rangle_{lmn}^m$ ,  $\langle \delta^2 \rangle_{lmn}^{lm}$  by Fourier inverting their appropriate intensities, which is performed by program COEFFS. All of these programs are listed in the appendix. Since fundamental peaks are present in the volume in which the diffuse scattering is measured, they appear after the separation in the local-order component. Thus, before the alphas can be computed the fundamental intensities present have to be removed. This was accomplished by assuming that the short range order intensity vanishes at the Bragg positions and extrapolating the short-range order intensity smoothly through these regions. The short range order coefficients thus obtained is finally used in the Williams (13) program to simulate the atomic configuration present in the disordered, and after 5 and 10 minutes ageing at 650°C.

The Williams (13) program uses 8000 atoms for the simulation and the composition of the alloy fixes the number of 1's ( $X_A$ ) and 0's ( $X_B$ ) present in the entire model. These atoms are interchanged until the alphas calculated for each site move towards the desired value, i.e. the experimentally observed values. This is done by examining individual

sites and not changing any site which would cause the composition to fall outside prescribed limits. Provided this criterion is met, a site is changed if the vector sum of the alphas moves closer to the design value. This program differs from Gehlen and Cohen's (12) program in the manner in which it examines the sites. The pairs to be interchanged are selected at random in Gehlen and Cohen's program, while Williams' developed a method of scanning which allows the entire model to be scanned sequentially in such a manner that the neighbors of any given site are examined in a random fashion. This scheme is faster and insures that each site is examined. The input data for Williams' program are the first three alphas, the overall composition of the alloy and the range within which the composition is allowed to vary. Once the model has been generated in the computer, any predetermined number of alphas may be calculated and printed. The resulting atomic configurations on successive (100) planes of the model are then printed out.

## CHAPTER IV

## RESULTS AND DISCUSSION

The measured diffuse intensity for the as-quenched alloy is shown in Figure 2a-f for the six planes in the fcc volume. The intensities are in Laue Monotonic units having been previously corrected for Compton scattering and nickel resonance x-rays (25). The diffuse peaks occur at  $(1, \frac{1}{2}, 0)$  and their equivalent positions in reciprocal space. The contours show that the peaks are very broad and spread over a large volume in reciprocal space with tails extending approximately 10 degrees on either side of the peak. The peaks are not very symmetrical due to the size effect intensity. The intensity distribution for plane 1 is similar to that obtained by Spruiell et al (3).

The superlattice reflections of  $\text{Ni}_4\text{Mo}$  occur at positions different than the diffuse peaks. These positions are shown by astericks on Figure 2a and 3a. The diffuse scattering contours do not appear to be affected by any intensity at the superlattice peak positions.

Okamoto (5) studied as-quenched  $\text{Ni}_4\text{Mo}$  using electron diffraction techniques. He plotted the diffracted intensity obtained along the  $[420]$  direction on  $(121)$  planes and observed small intensity maxima at superlattice peak positions. He claims this as evidence for ordered domains existing in the as-quenched alloy. Since the volume in which our measurements were made does not include a large section of the  $(121)$  plane, this could not be checked thoroughly. Instead, the intensity distribution along the  $[420]$  direction on the  $(100)$  plane is shown in Figure 4.

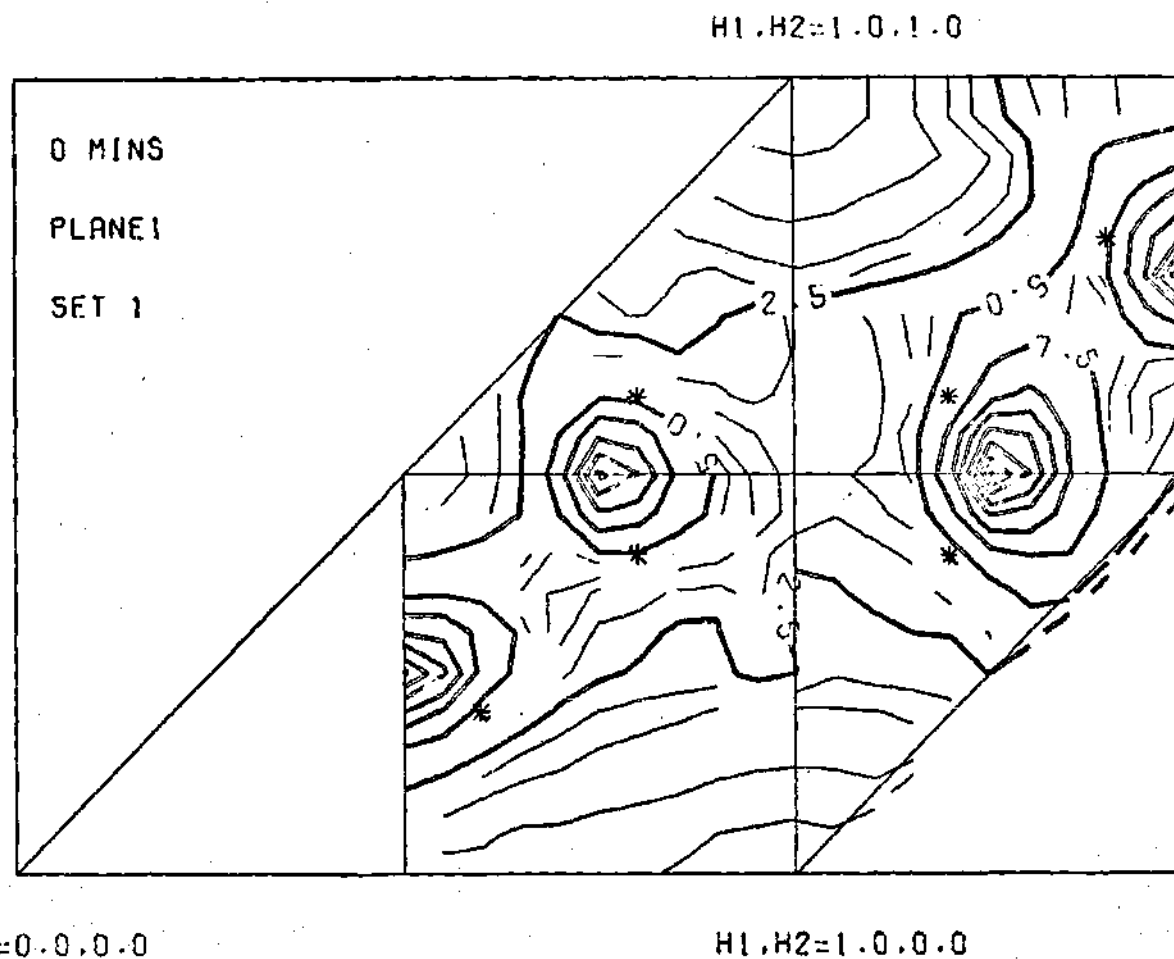
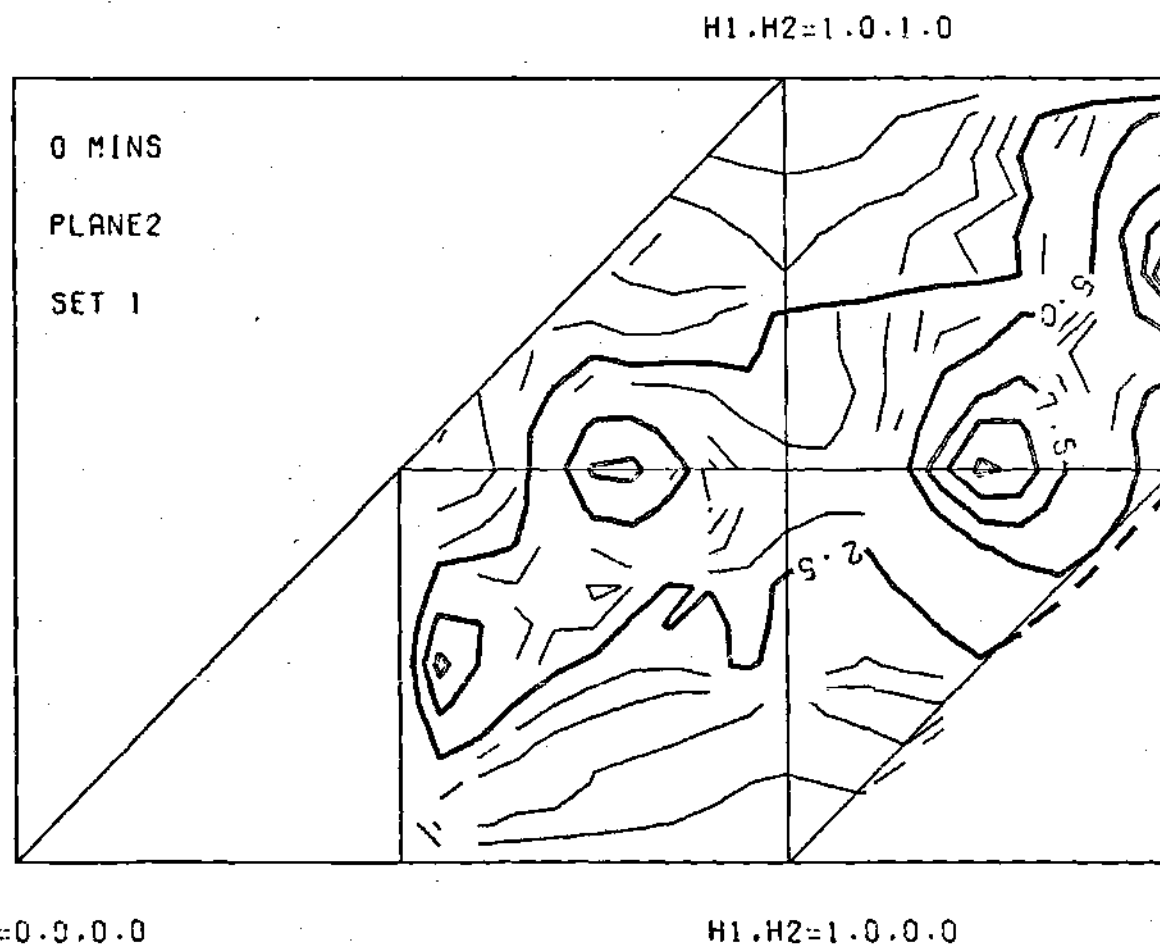


Figure 2a. Diffuse Intensity Distribution on the ( $h_1, h_2, h_3 = 0.00$ ) Plane of Reciprocal Space for as-quenched  $\text{Ni}_4\text{Mo}$ . (Quantity Plotted is  $\frac{1}{N} \sum_{\mathbf{A}} \sum_{\mathbf{B}} (f_{\mathbf{A}} - f_{\mathbf{B}})^2$ . Contours Near Fundamental Bragg Reflections Have Been Removed.)



**Figure 2b.** Diffuse Intensity Distribution on the ( $h_1, h_2, h_3 = 0.05$ ) Plane of Reciprocal Space for as quenched  $\text{Ni}_4\text{Mo}$ . Quantity Plotted is  $I_{\text{eu}}/N X_A X_B (f_A - f_B)^2$ . (Contours Near Fundamental Bragg Reflections Have Been Removed)

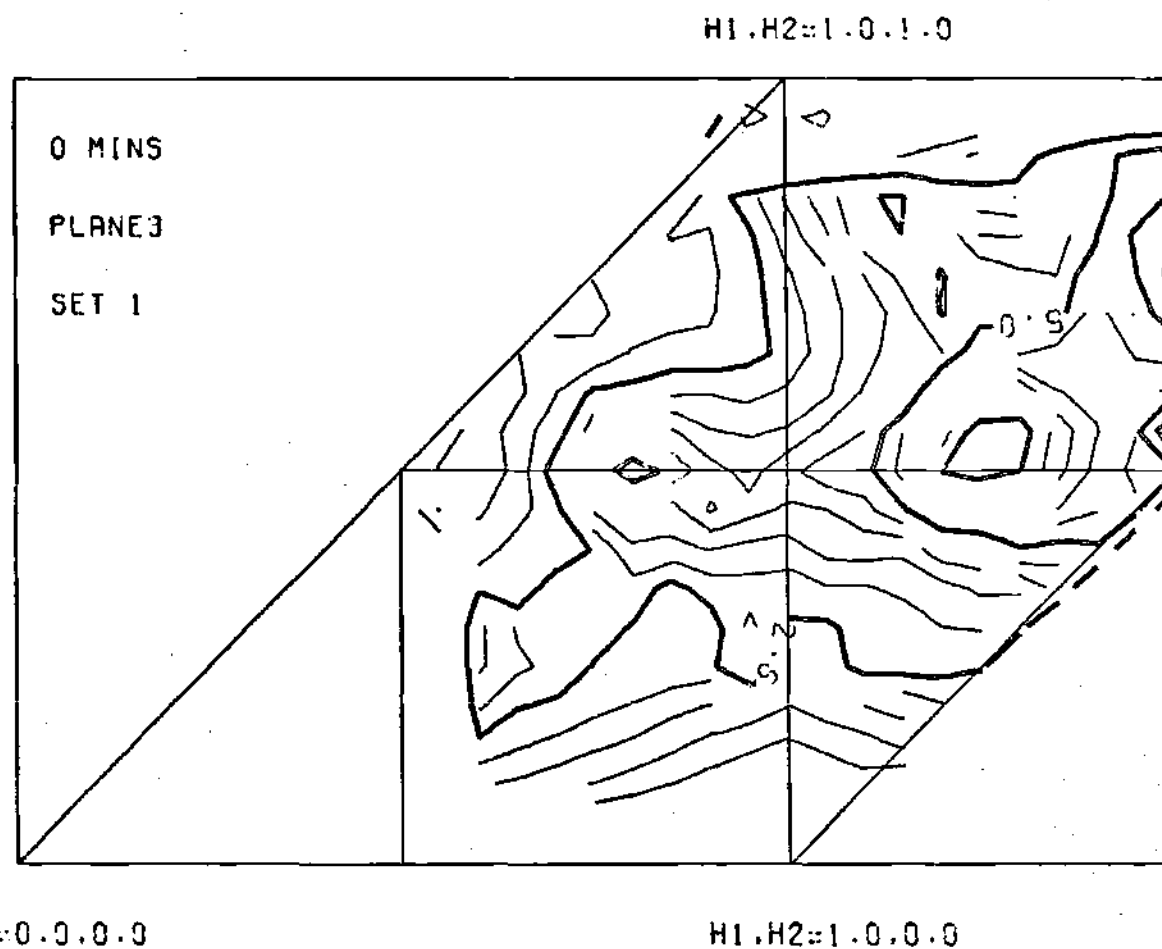
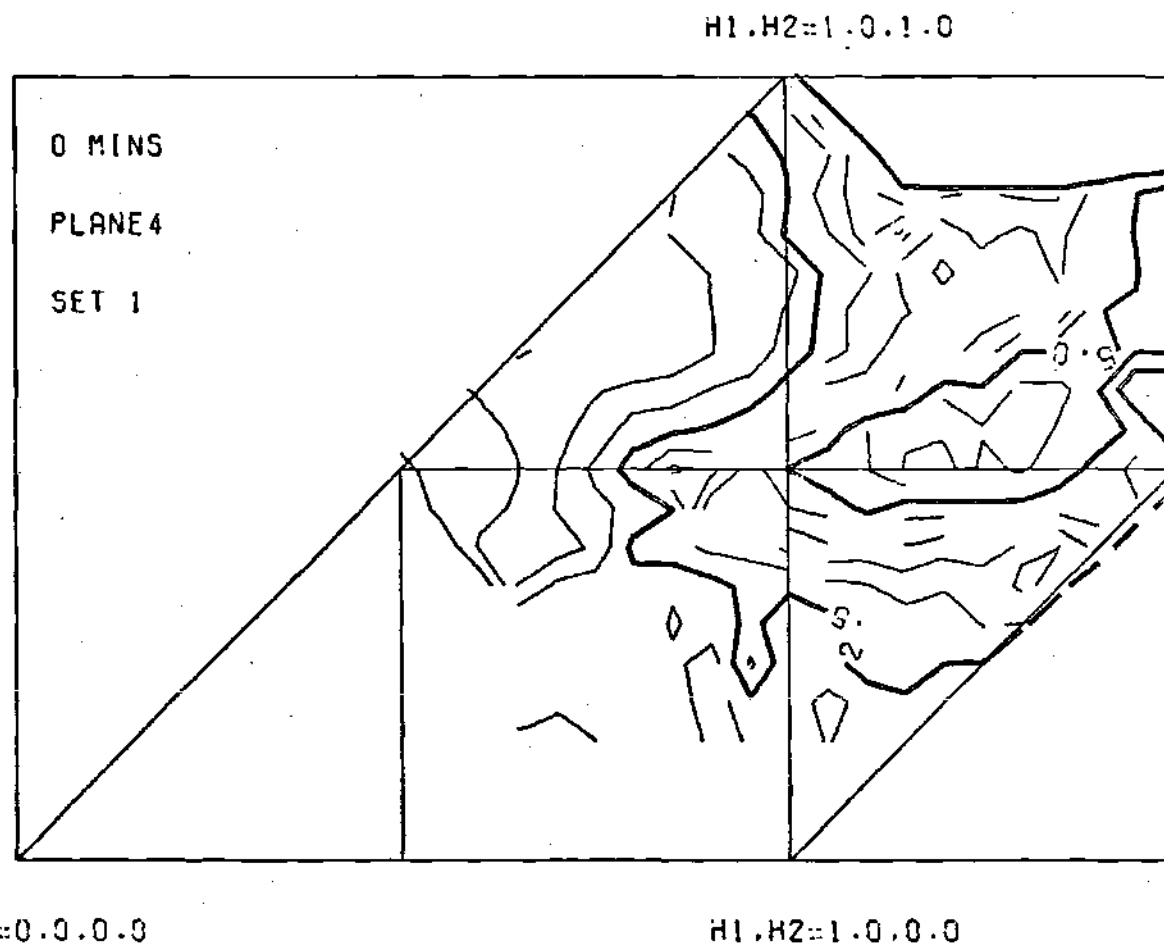
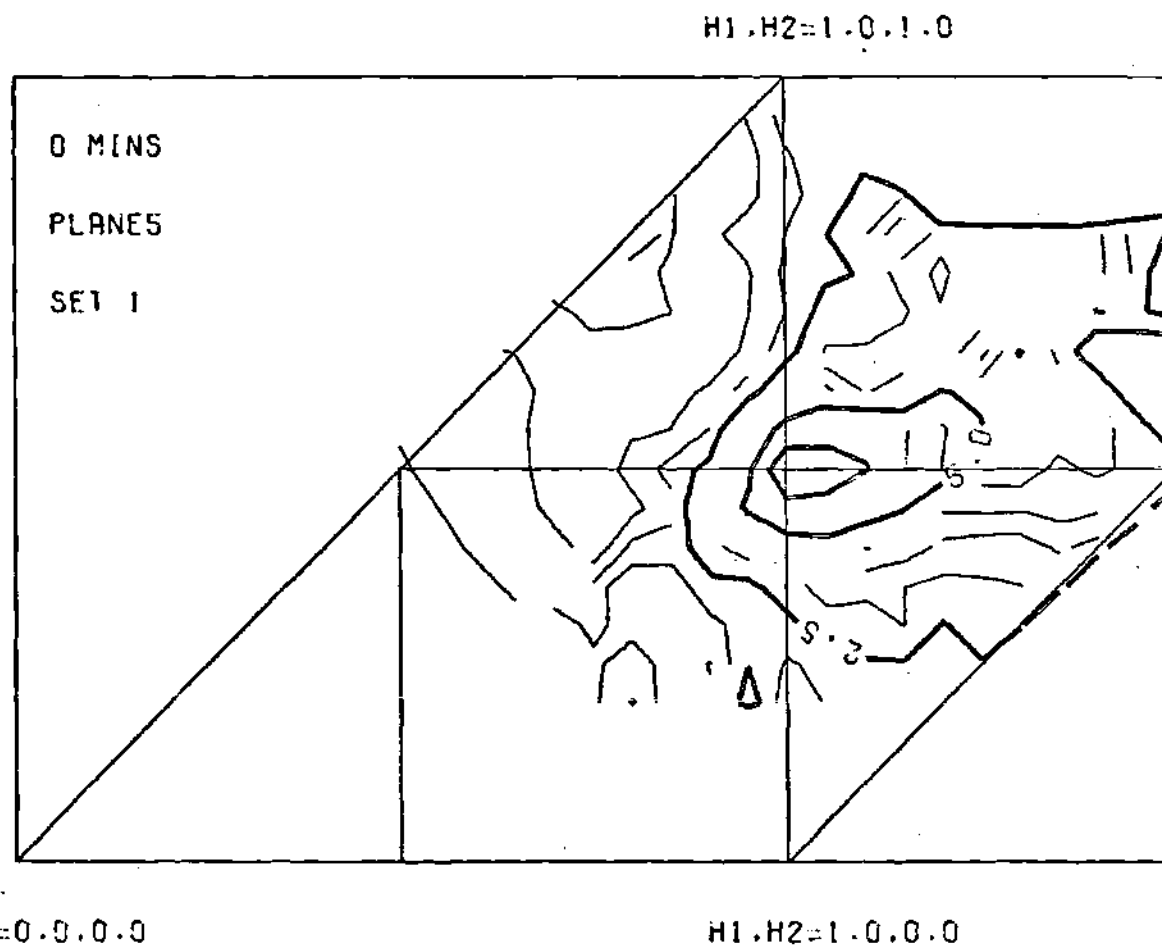


Figure 2c. Diffuse Intensity Distribution on the  $(h_1, h_2, h_3 = 0.10)$  Plane of Reciprocal Space for as quenched Nickel - 20 at. % Molybdenum Alloy. (Quantity Plotted is  $I_{\text{eu}}/N X_A X_B (f_A - f_B)^2$ . Contours Near Fundamental Bragg Reflections Have Been Removed).



**Figure 2d.** Diffuse Intensity Distribution on the ( $h_1, h_2, h_3 = 0.15$ ) Plane of Reciprocal Space for as quenched Nickel - 20 at. % Molybdenum Alloy. Quantity Plotted is  $I_{\text{eu}}/N_X X_A X_B (f_A - f_B)^2$ . (Contours Near Fundamental Bragg Reflections Have been Removed.)



**Figure 2e.** Diffuse Intensity Distribution on the  $(h_1, h_2, h_3 = 0.20)$  Plane of Reciprocal Space for as quenched Nickel - 20 at. % Molybdenum Alloy. (Quantity Plotted is  $I_{eu}/N X_A X_B (f_A - f_B)^2$ . Contours Near Fundamental Bragg Reflections Have Been Removed).



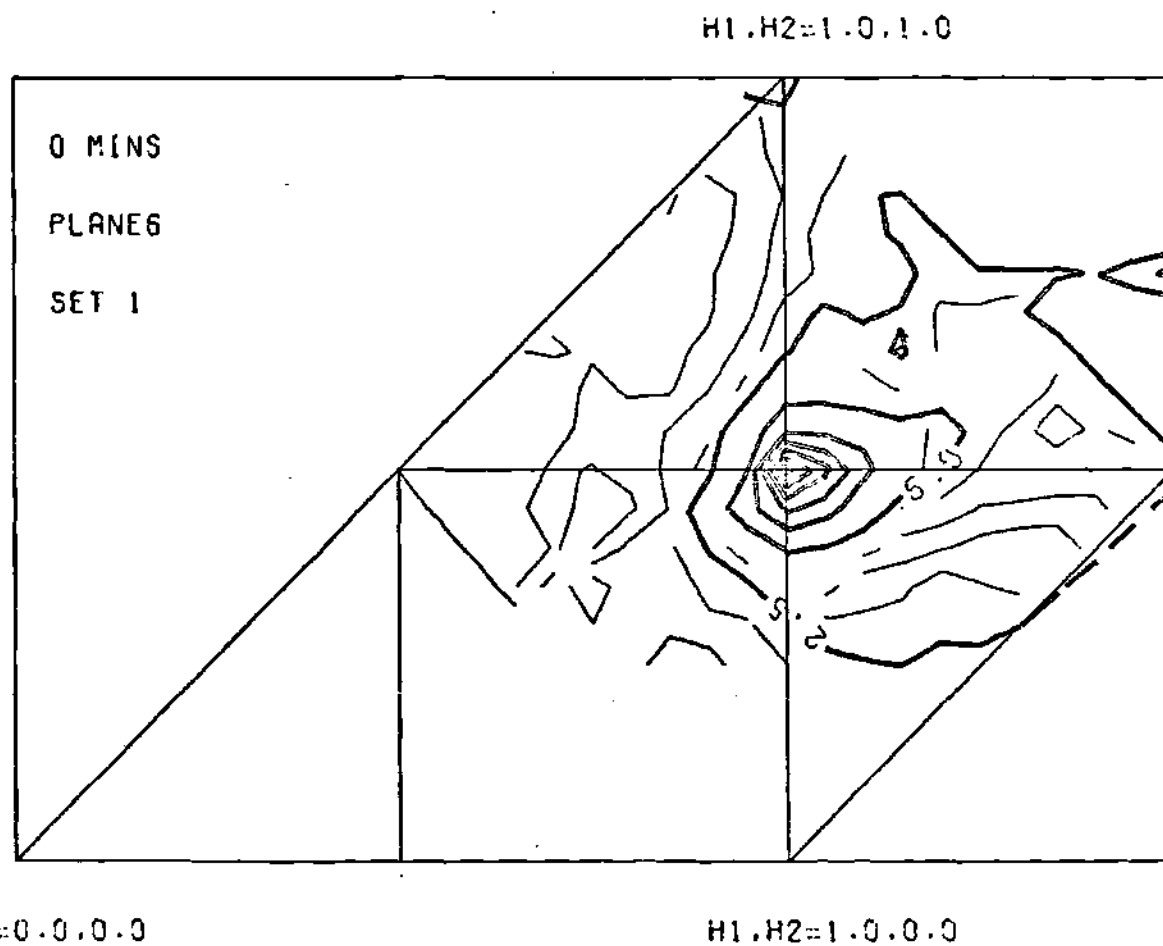


**Figure 2f.** Diffuse Intensity Distribution on the  $(h_1, h_2, h_3 = 0.25)$  Plane of Reciprocal Space for as quenched  $\text{Ni}_4\text{Mo}$ . (Quantity Plotted is  $I_{\text{eu}}/N_X \sum_A \sum_B (f_A - f_B)^2$ . Contours Near Fundamental Bragg Reflections Have Been Removed).

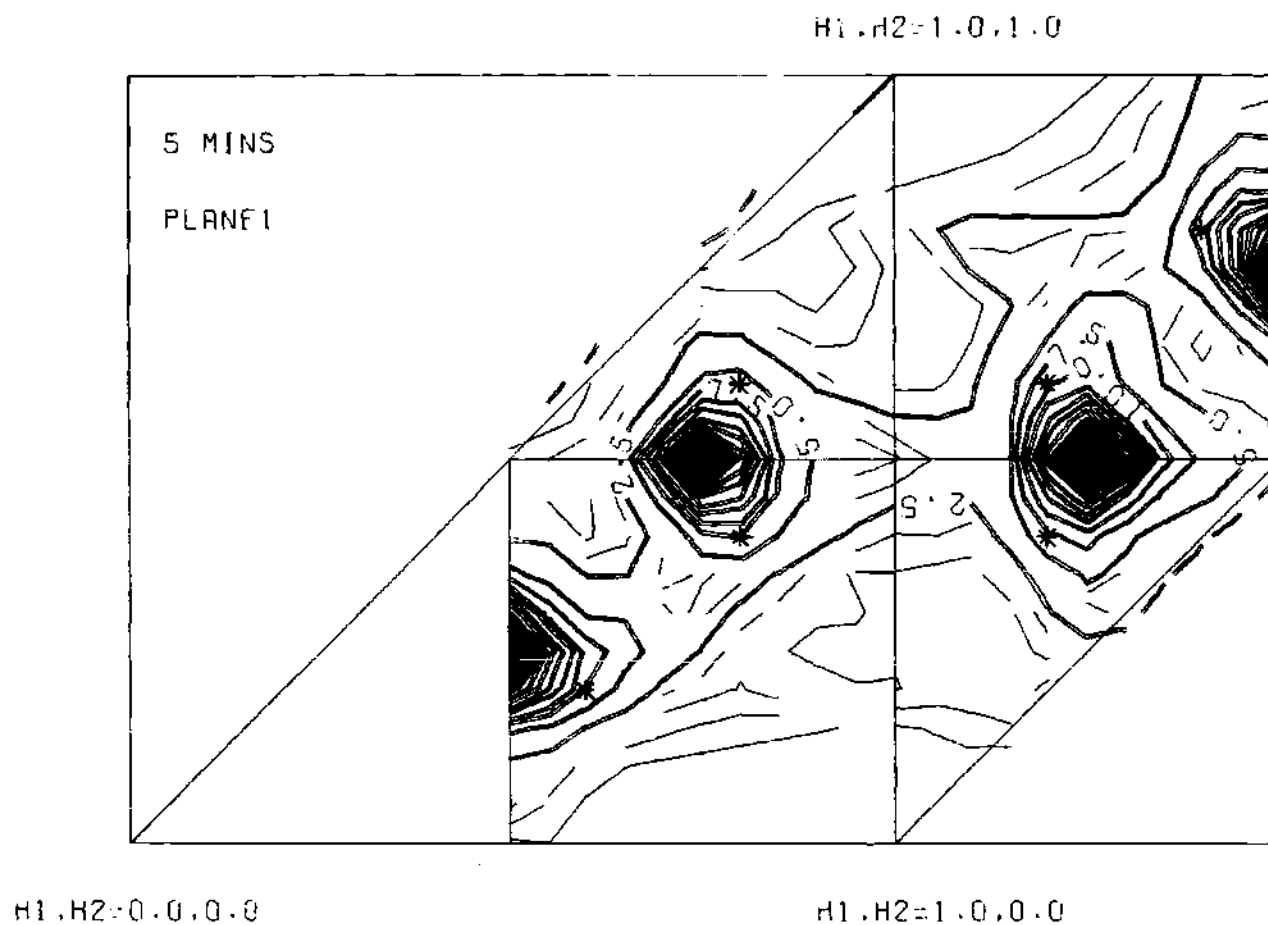


Figure 3a. Diffuse Intensity Distribution on the ( $h_1, h_2, h_3 = 0.00$ ) Plane of Reciprocal Space for 5 mins. Ordered Nickel - 20 at.% Molybdenum Alloy. (Quantity Plotted is  $I_{\text{eu}}/N X_A X_B (f_A - f_B)^2$ . Contours Near Fundamental Bragg Reflections Have Been Removed).

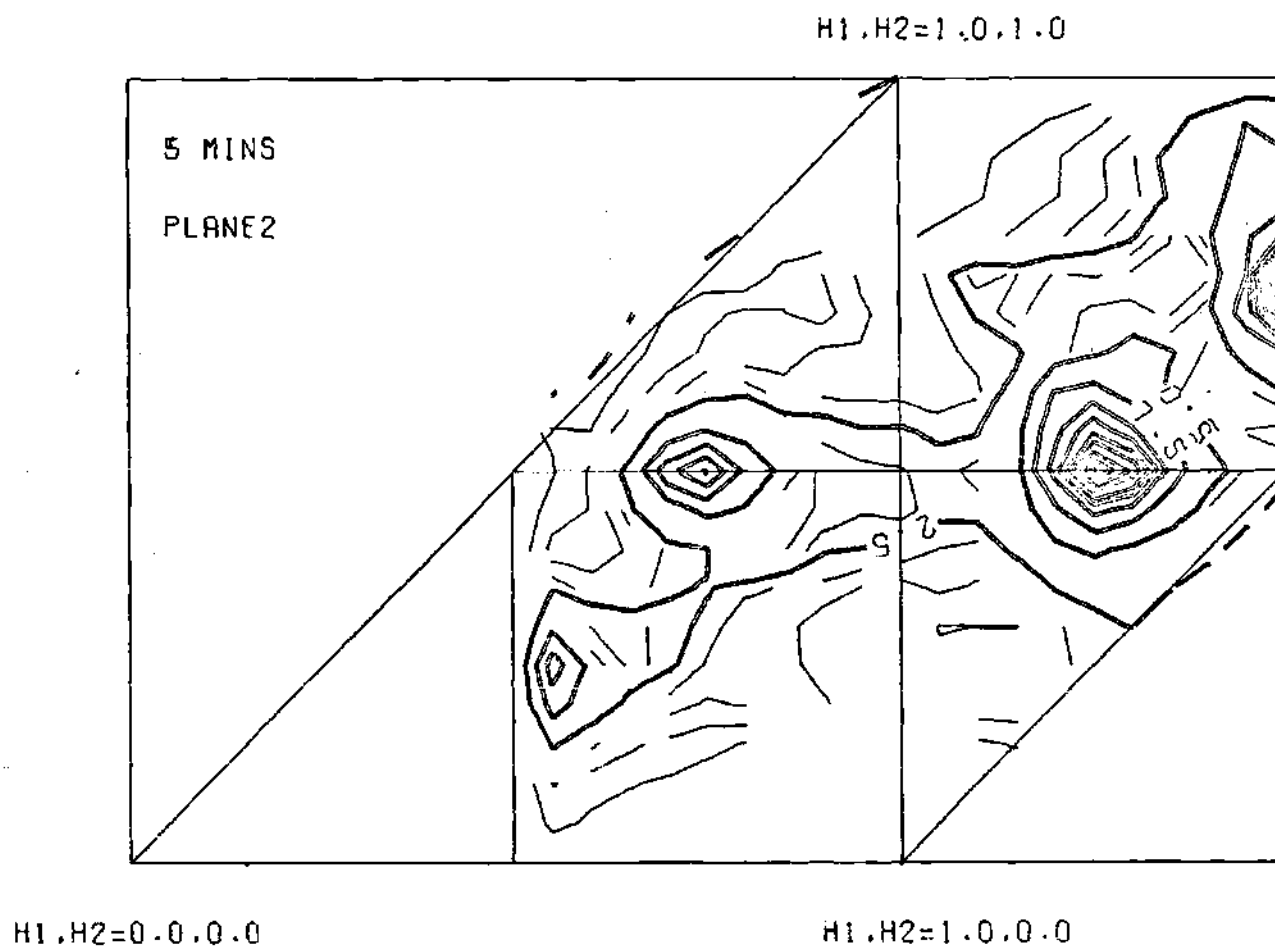


Figure 3b. Diffuse Intensity Distribution on the ( $h_1, h_2, h_3 = 0.05$ ) Plane of Reciprocal Space for 5 mins. Ordered Nickel - 20 at. % Molybdenum Alloy. (Quantity Plotted is  $I_{eu}/N X_A X_B (f_A - f_B)^2$ . Contours Near Fundamental Bragg Reflections Have Been Removed).

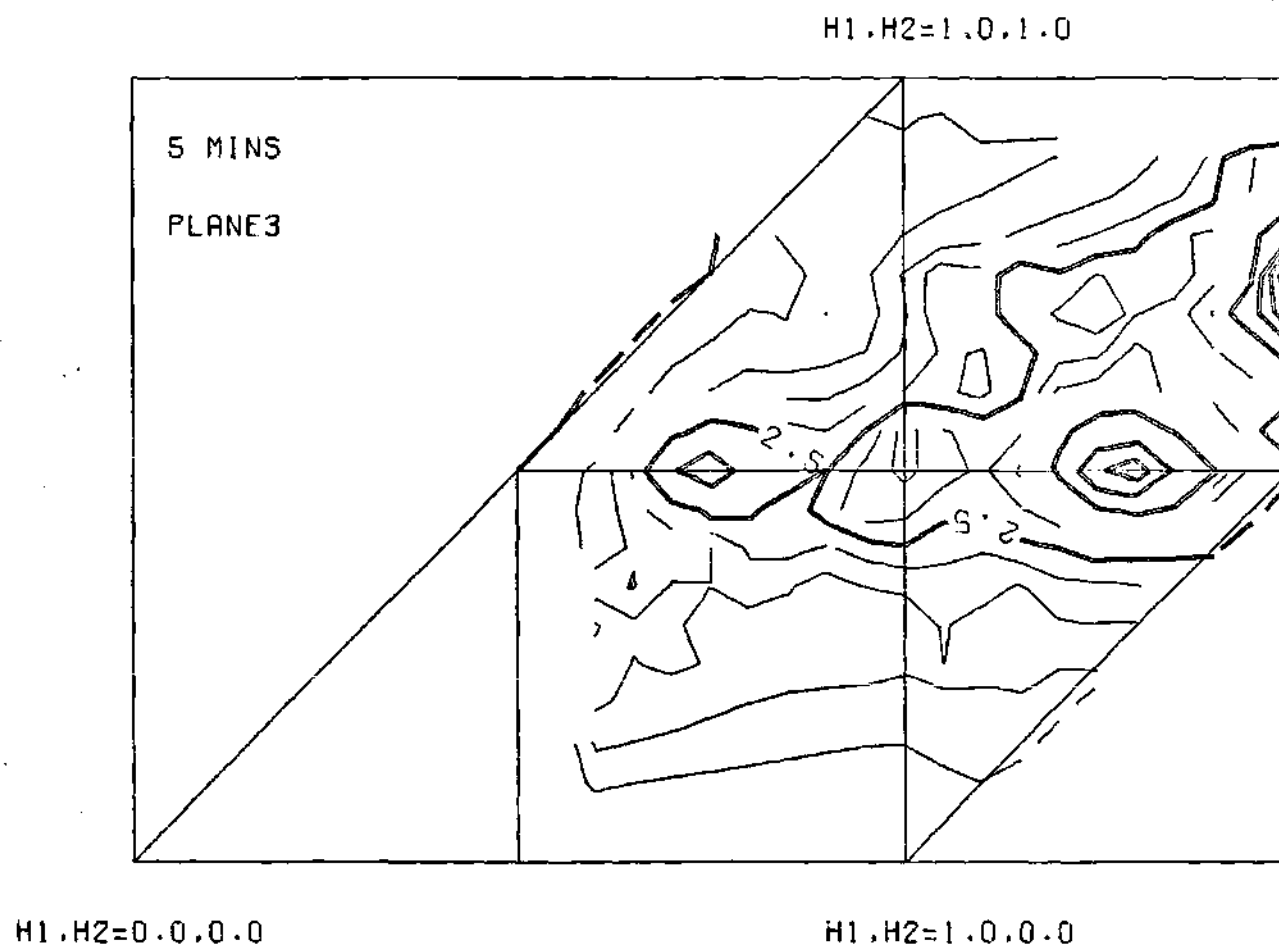


Figure 3c. Diffuse Intensity Distribution on the  $(h_1, h_2, h_3 = 0.10)$  Plane of Reciprocal Space for 5 mins. Ordered Nickel - 20 at. % Molybdenum Alloy. (Quantity Plotted is  $I_{\text{eu}}/N X_A X_B (f_A - f_B)^2$ . Contours Near Fundamental Bragg Reflections Have Been Removed).

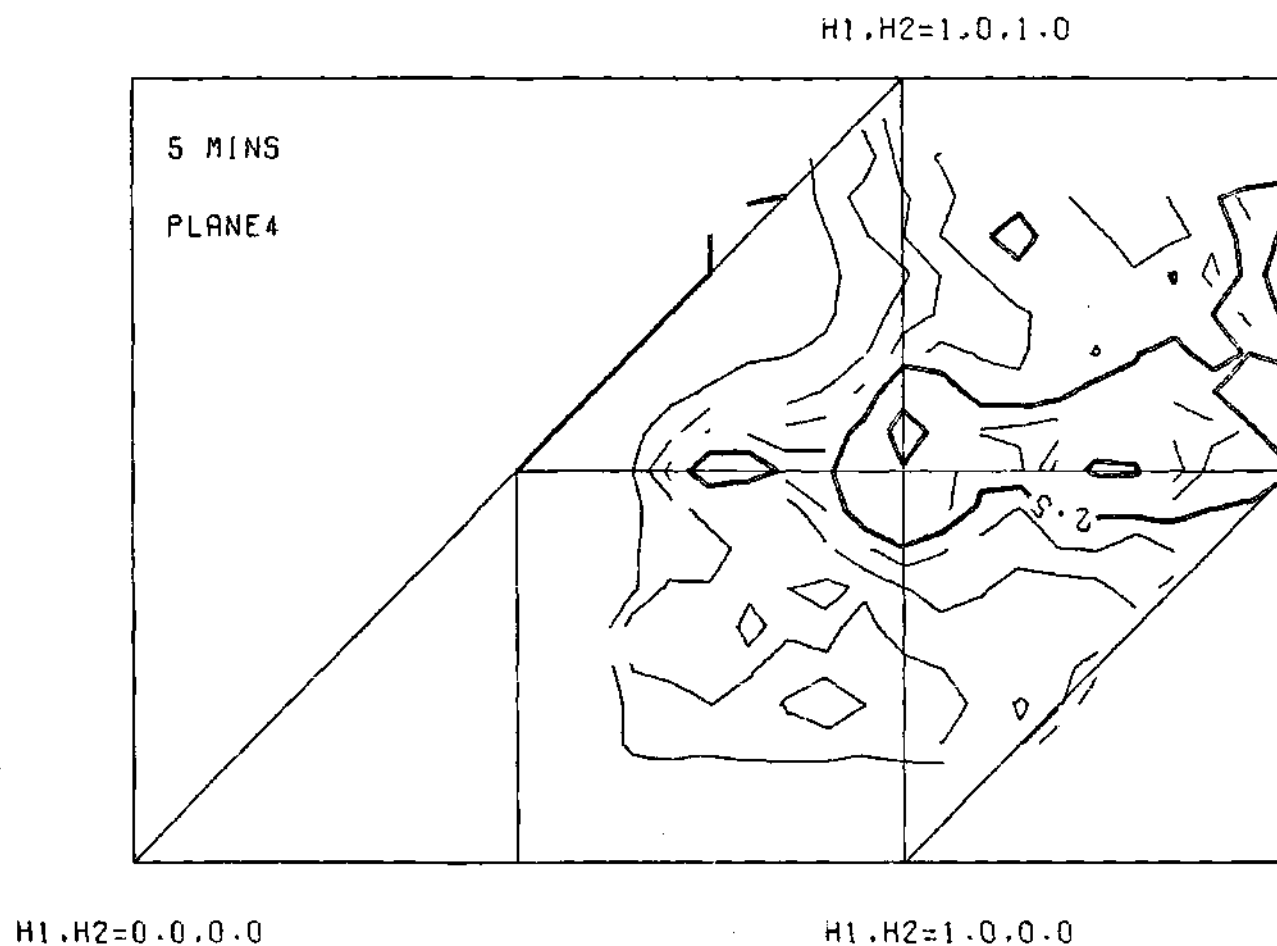


Figure 3d. Diffuse Intensity Distribution on the  $(h_1, h_2, h_3 = 0.15)$  Plane of Reciprocal Space for 5 mins. Ordered Nickel - 20 at. % Molybdenum Alloy. (Quantity Plotted is  $I_{\text{eu}}/N X_A X_B (f_A - f_B)^2$ . Contours Near Fundamental Bragg Reflections Have Been Removed).





Although the (100) planes are not the most suitable for observation of superlattice intensities, it can be seen that small maxima do occur at superlattice peak positions, and these maxima are simply due to the diffuse peak tails. These are not due to any other intensities as can be seen from the 3D map of Figure 5.

On ordering the alloy for 5 minutes at  $650^{\circ}\text{C}$ , the diffuse peaks sharpen considerably and the peak intensity increases by approximately threefold, Figure 3a-f. It is interesting to compare the (002) electron diffraction pattern, Figure 6b, of reference 5 and our Figure 3a, since they are supposed to represent the same state of order (heat treated for 5 minutes at  $650^{\circ}\text{C}$ ). The diffuse intensity distribution present in the electron diffraction pattern of reference 5 is shown schematically in Figure 6, where each diffuse spot is related to its superlattice peak by a "paddle shaped" intensity distribution. An examination of Figure 3a where the superlattice peak positions are marked by astericks shows no clear cut "paddle shaped" intensity. Since the manner by which the ordering was performed was different (in our case, the sample was encapsulated in a quartz tube under vacuum and heated in a furnace, whereas Okamoto heat-treated small disc-like samples in a salt bath at  $650^{\circ}\text{C}$ ), the state of order considered might be different. The intensity distribution of Figure 6b of reference 5 shows a stage of ordering far advanced, whereas Figure 3a shows an earlier stage. The intensity distribution obtained for the sample ordered 10 minutes at  $650^{\circ}\text{C}$  is similar to the 5 minutes ordered case, except that the peak intensities are slightly higher. Plots of the measured diffuse intensity for the 10 minutes ordered sample are given in the appendix.



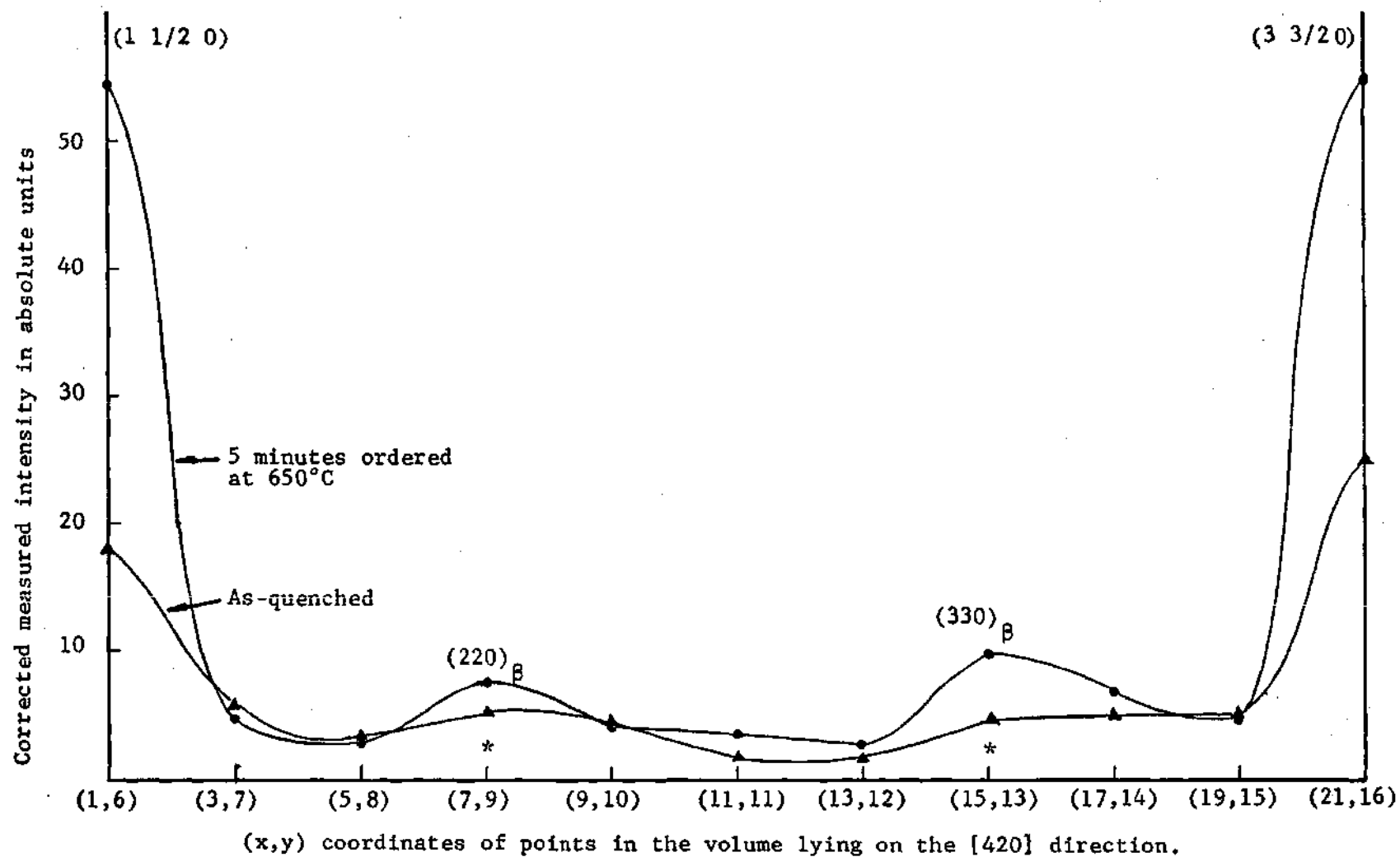


Figure 4. Plot of Corrected measured Intensity Along [420] Direction on (100) Plane. (Astericks marks positions of superlattice peak positions).

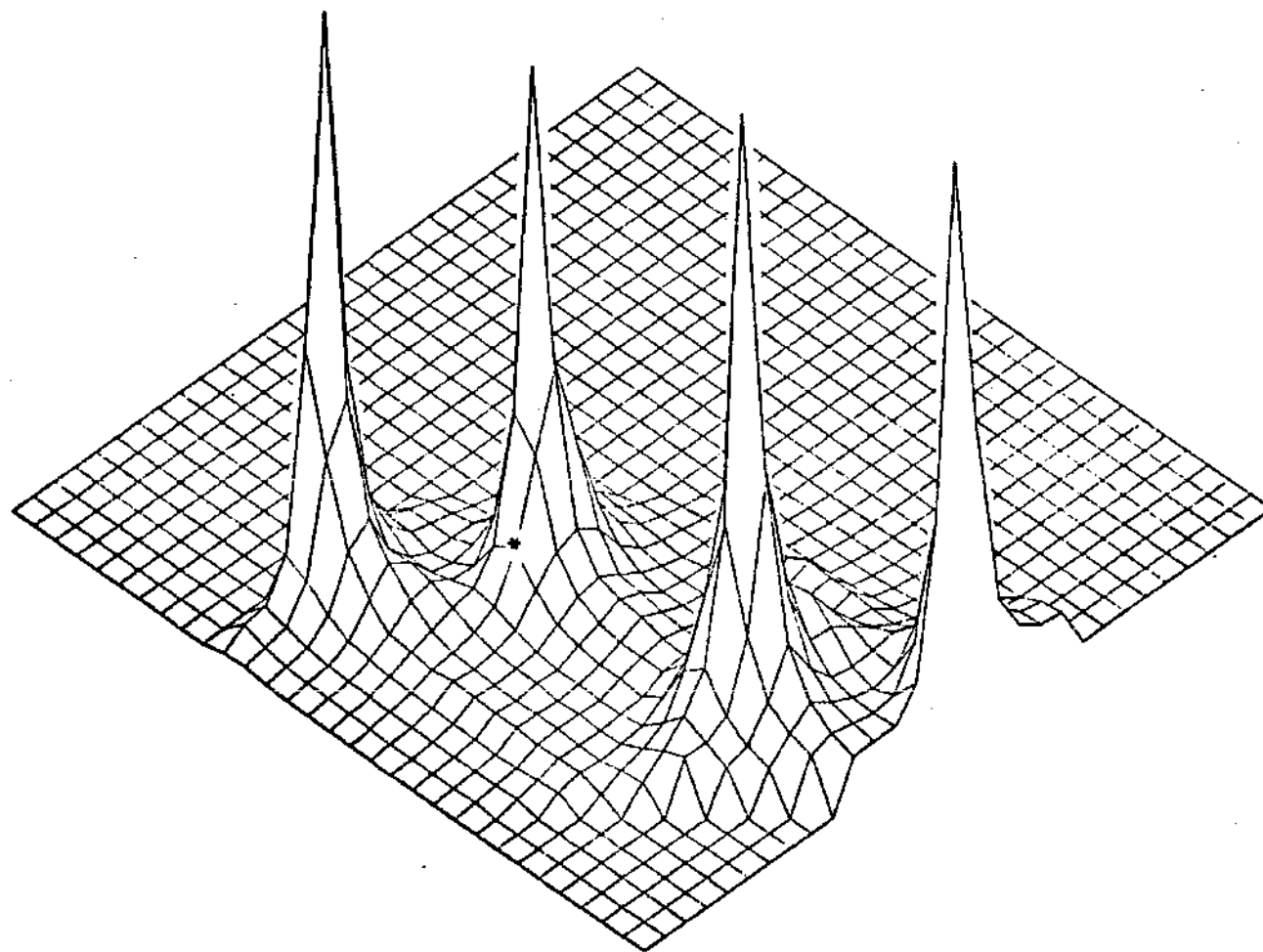


Figure 5. 3D Map of Measured Diffuse Intensity on the  $(h_1, h_2, h_3 = 0.0)$  Plane of  $\text{Ni}_4\text{Mo}$  Ordered for 5 mins. at  $650^\circ\text{C}$ . (Asterick shows position of superlattice reflection).

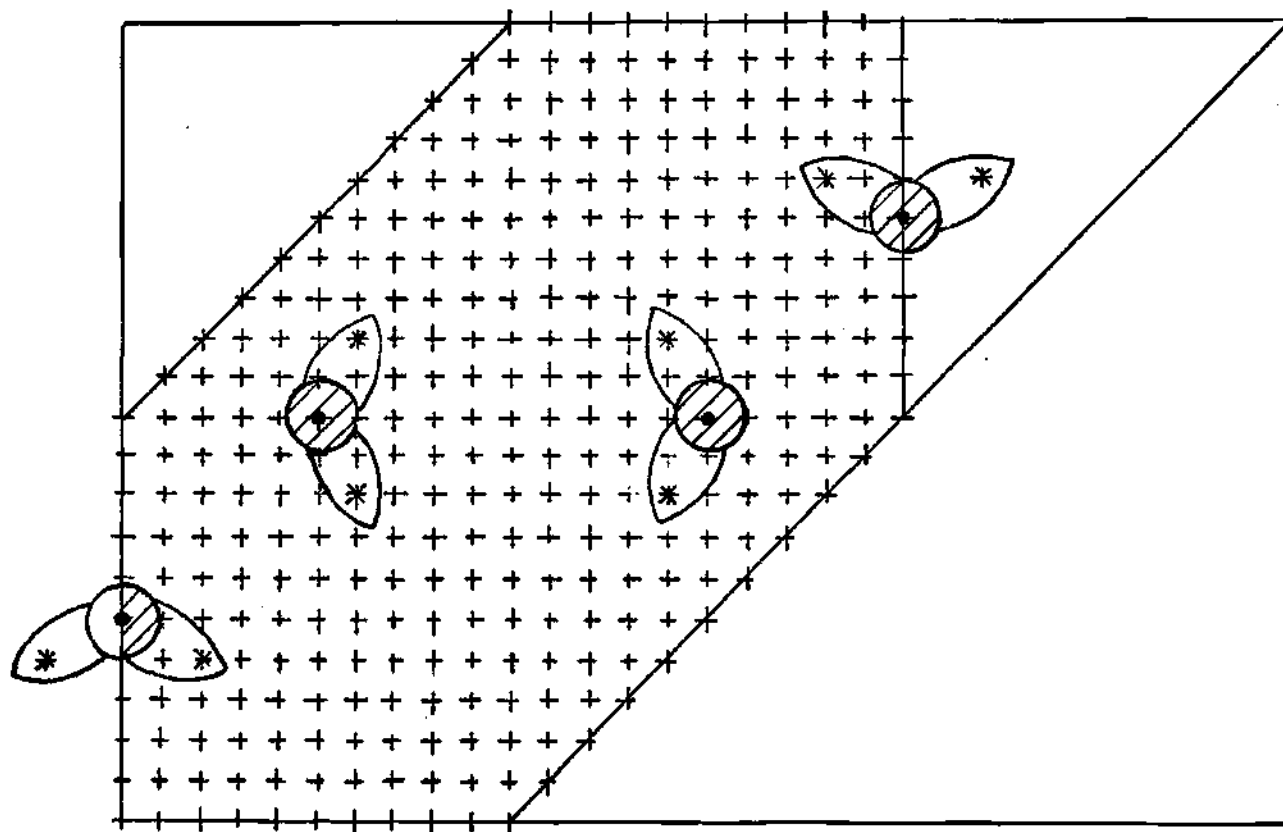


Figure 6. A Schematic of the Intensity Distribution on the (200) Plane of  $\text{Ni}_4\text{Mo}$  as Shown by reference (5). (Astericks marks positions of superlattice peaks).

The measured intensities were separated into the different components using the program SEPRIT, which gives the separated components in their respective repeat volumes. The short range order intensity obtained after separation of the "size effect" for the as-quenched alloy is shown in Figure 7a-f. The intensity distribution is symmetrical about the diffuse peak positions. The coefficients,  $\alpha_{lmn}^m$ ,  $\gamma_{lmn}^m$ ,  $\langle \phi^2 \rangle_{lmn}^m$ ,  $\langle \phi^2 \rangle_{lmn}^{1m}$  are obtained by Fourier inversion using the repeat volumes and their respective symmetries for the different components. The  $\delta$  coefficients represent the combined first order TDS and second order static displacement terms. These coefficients, for the as-quenched and slightly-ordered cases, have been added in the appendix. These coefficients decrease with increasing order.

Table 2 gives the three-dimensional local order parameters obtained from the separated short-range order component for the three different cases. The coefficients were checked by synthesizing the local-order intensities and recalculating the alphas from the synthesized intensity. The round off error was less than one percent. Since the ordered peaks were fairly sharp, alphas up to (888) were used to synthesize the intensity.  $\alpha_{000} = 1.587$  for the as-quenched alloy although theoretically the value should be 1.000. A disagreement of this magnitude is common in the literature on diffuse scattering measurements, although the reason is unclear. Gragg (20) has shown from theoretical error analysis that about 20 percent of the error in  $\alpha_{000}$  can be attributed to the noninclusion of displacement effect terms higher than second order. The extra unaccountable intensity might arise from resonance x-rays (25) and affects the lower order coefficients the most.

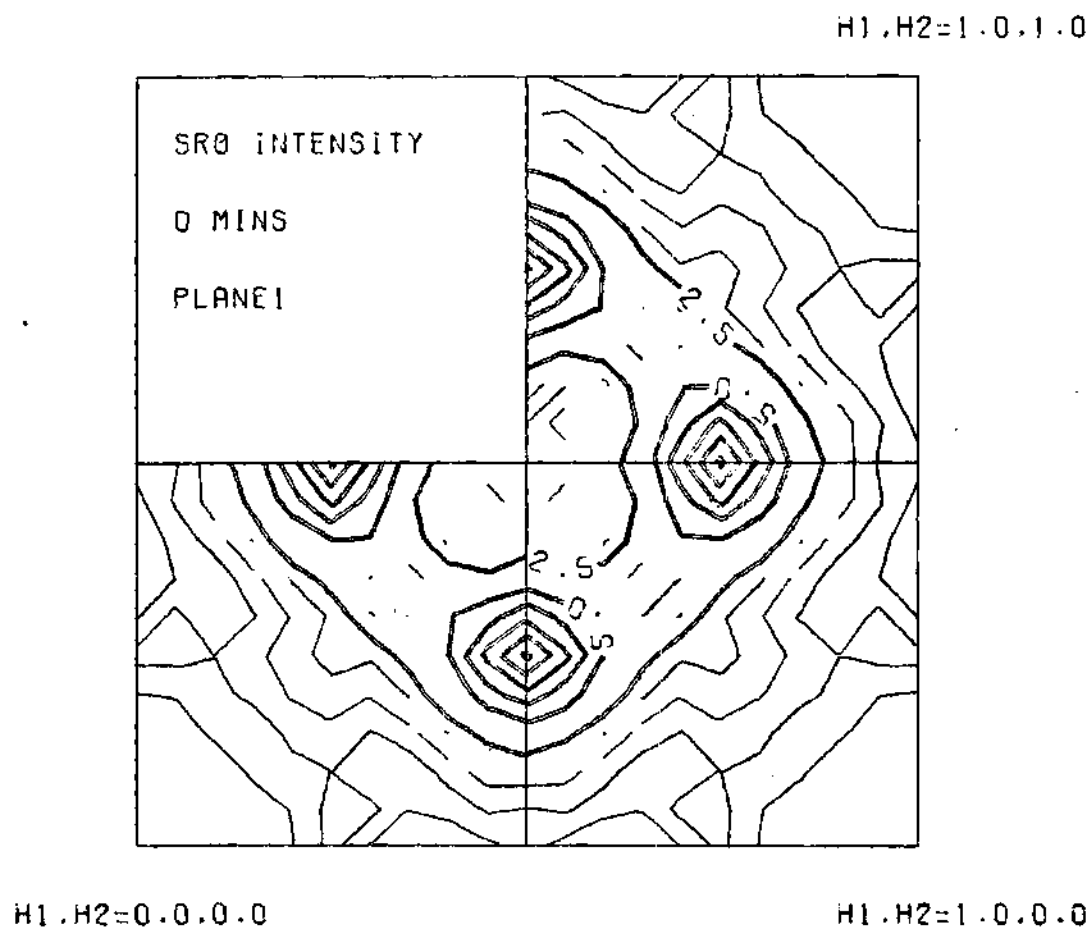


Figure 7a. Distribution of the Separated Short Range Order Intensity in the First Quadrant in Reciprocal Space. (Quantity Plotted is same as in Figure 2. ( $h_3 = 0.00$ )).

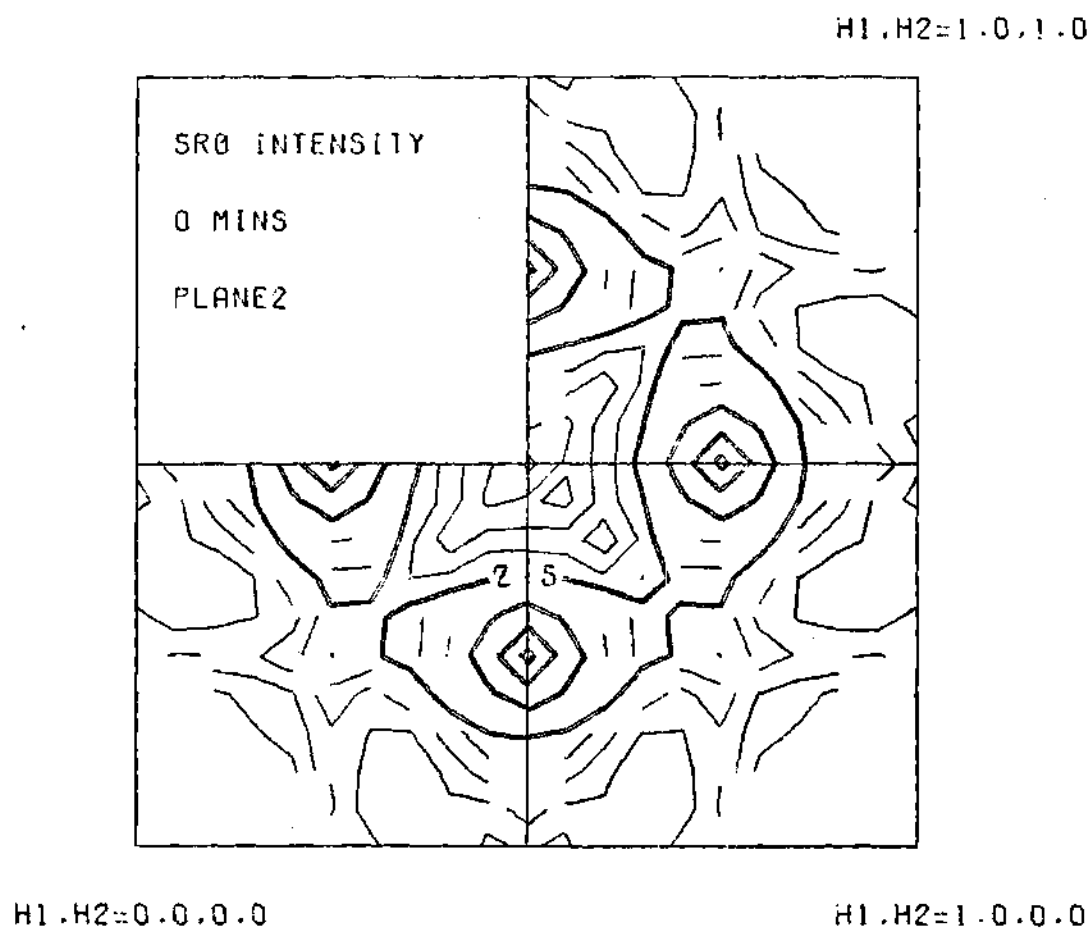


Figure 7b. Distribution of the Separated Short Range Order Intensity in the First Quadrant in Reciprocal Space. (Quantity Plotted is same as in Figure 2. ( $h_3 = 0.05$ )).

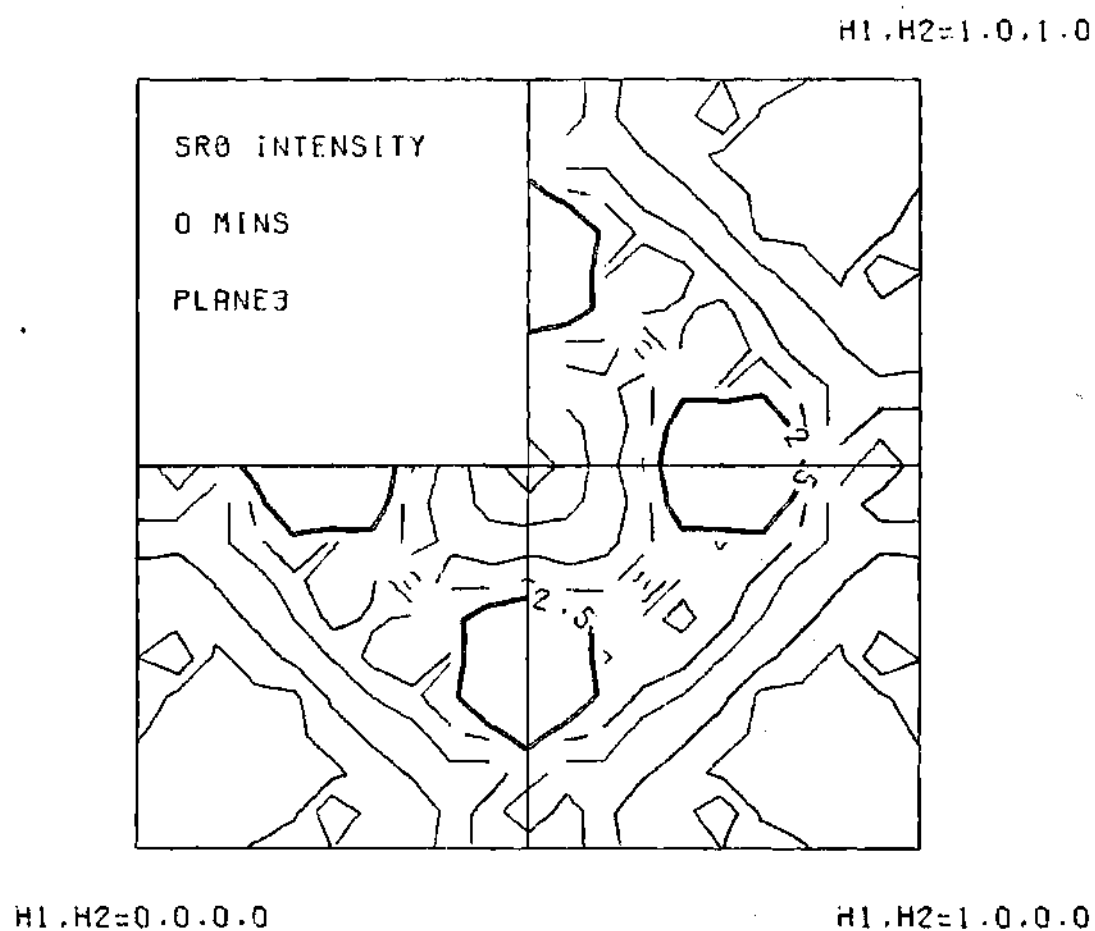


Figure 7c. Distribution of the Separated Short Range Order Intensity in the First Quadrant in Reciprocal Space. Quantity Plotted is same as in Figure 2. ( $h_3 = 0.10$ )).

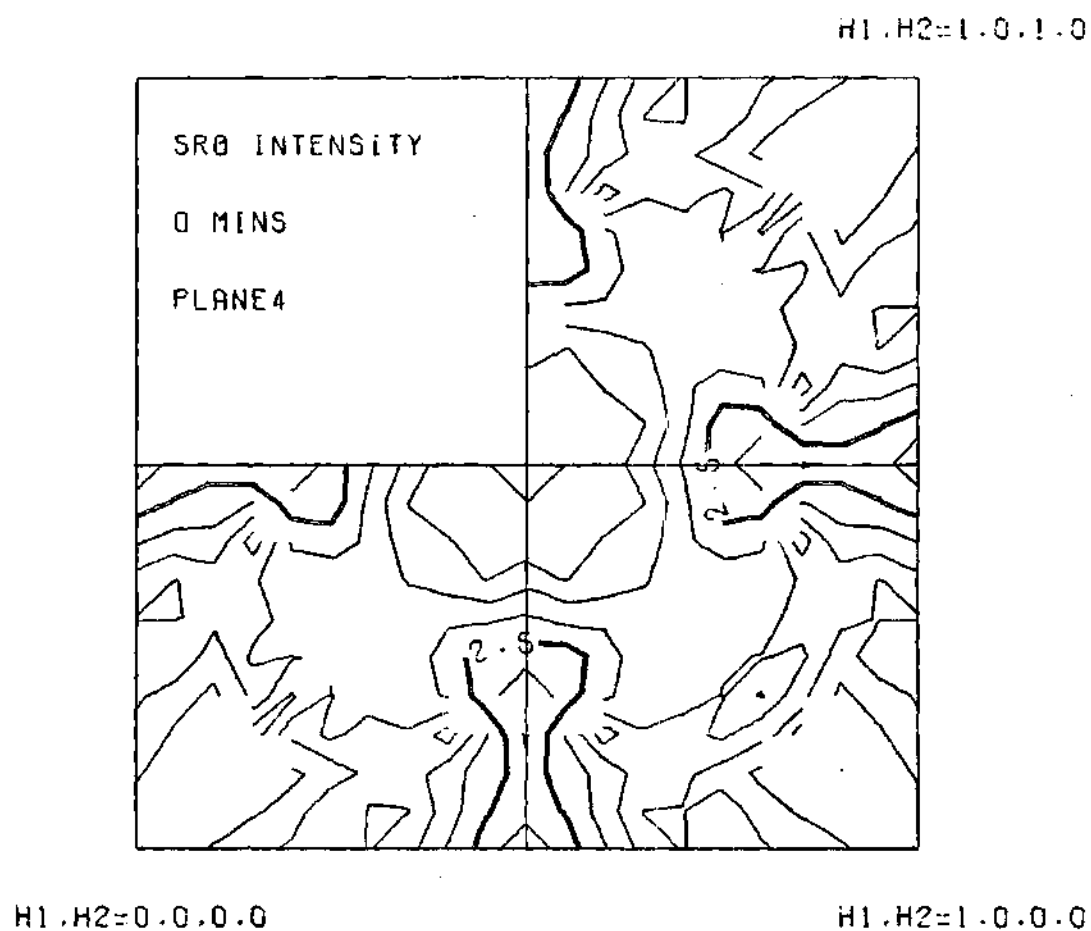


Figure 7d. Distribution of the Separated Short Range Order Intensity in the First Quadrant in Reciprocal Space. (Quantity Plotted is same as in Figure 2). ( $h_3 = 0.15$ ).



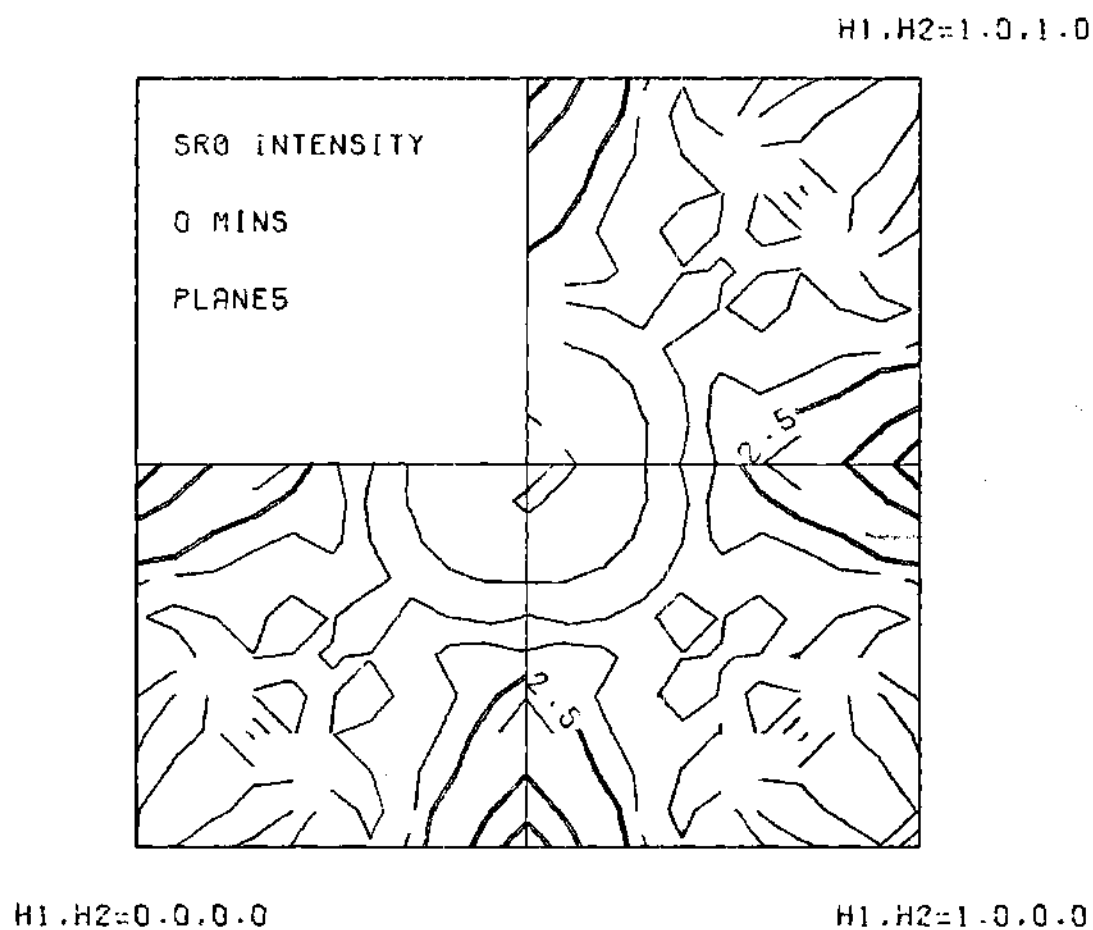


Figure 7e. Distribution of the Separated Short Range Order Intensity in the First Quadrant in Reciprocal Space. (Quantity Plotted is same as in Figure 2.) ( $h_3 = 0.20$ ).

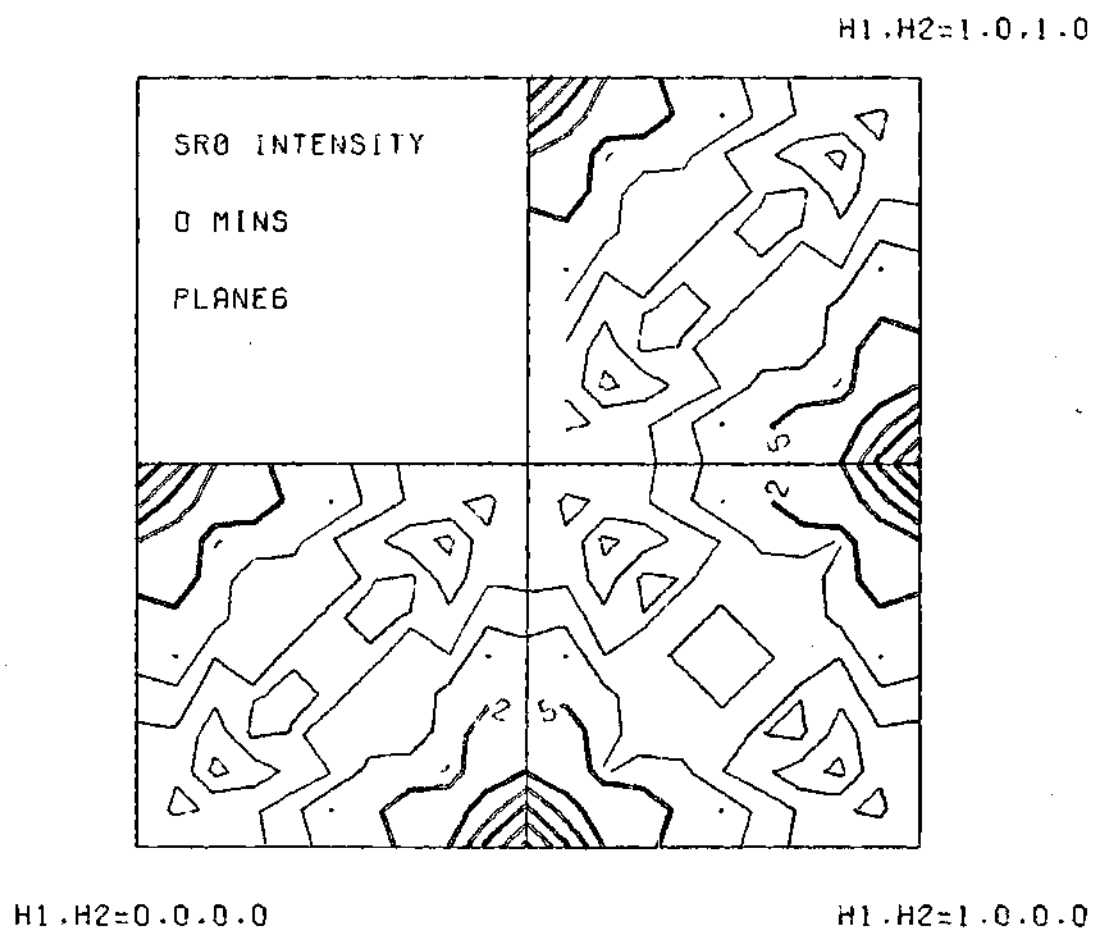


Figure 7f. Distribution of the Separated Short Range Order Intensity in the First Quadrant in Reciprocal Space. (Quantity Plotted is same as in Figure 2. ( $h_3 = 0.25$ )).

Table 2. Three Dimensional Short Range Order Coefficients for Nickel-20 Atomic Percent Molybdenum Alloy for Different Conditions As Shown.

LMN	AS-QUENCHED	ORDERED AT 650°C	
		for 5 mins.	for 10 mins.
000	1.587	1.489	1.173
110	-0.204	-0.243	-0.225
200	-0.010	0.112	0.107
211	0.114	0.170	0.155
220	-0.072	-0.186	-0.165
310	-0.064	-0.103	-0.074
222	-0.123	-0.180	-0.132
321	0.034	0.081	0.046
400	0.110	0.295	0.232
330	0.005	-0.045	-0.009
411	-0.046	-0.099	-0.066
420	0.035	0.042	0.028
332	0.013	0.016	0.019
422	-0.014	-0.036	-0.027
431	-0.019	-0.031	-0.023
510	-0.016	-0.047	-0.043
521	0.015	0.049	0.040
440	0.029	0.091	0.062
433	-0.011	-0.007	-0.006
530	-0.009	-0.031	-0.028
600	-0.025	-0.005	0.010
442	0.014	0.036	0.021

The SRO coefficients obtained were used to computer simulate an average atomic configuration for the alloy. Performing such a simulation with Williams (13) program for the as-quenched and 5 minutes ordered structure a model was obtained from which the SRO coefficients could be calculated. A comparison of the alphas obtained from the model and those measured is shown in Table 3 for the as-quenched and 5 minutes ordered alloy. The fit extends down to the higher order alphas and is consistent with the measured values in signs and magnitude. The model developed follows the large rise in  $\alpha_{200}$ , observed experimentally when the alloy was ordered slightly. In addition to generating the model and giving the relative positions of the two kinds of atoms in the model, the computer may be programmed to search the model for atoms or groups of atoms satisfying certain specified criteria. This information produces a better insight and understanding of the model. Tables 4-5 give some information of this type for the as-quenched alloy. Table 4 gives the number of molybdenum neighbors in the first and second shell for each Mo atom in a random alloy. Table 5 lists similar information for the model of the as-quenched alloy. There are 23 molybdenum atoms having no first Mo neighbors and 2 second nearest Mo neighbors in the random alloy, while this number increases to 279 for the as-quenched alloy. Physically this means that "clusters" form.

To obtain a better concept of the local order it is useful to try to isolate regions in the model which meets a specified criterion and to examine the size and shape of such regions. Various authors (3,5,8,9) have argued that the as-quenched condition in  $\text{Ni}_4\text{Mo}$  consists of microdomains of LRO, so this possibility was examined. Each

Table 3. Comparison of the Three Dimensional Short Range Order Coefficients as Obtained from the Computer Generated Model with those Measured for the As-Quenched and 5 Minutes at 650°C Order Sample.

LMN	AS-QUENCHED		5 MINS ORDERED	
	Measured	Model	Measured	Model
000	1.587	1.000	1.489	1.000
110	-0.204	-0.185	-0.243	-0.204
200	-0.010	-0.006	0.112	0.110
211	0.114	0.120	0.170	0.151
220	-0.072	-0.070	-0.186	-0.168
310	-0.064	-0.027	-0.103	-0.090
222	-0.123	-0.123	-0.180	-0.188
321	0.034	0.013	0.081	0.072
400	0.110	0.110	0.295	0.296
330	0.005	0.005	-0.045	-0.040
411	-0.046	-0.046	-0.099	-0.089
420	0.035	0.029	0.042	0.054
332	0.013	0.024	0.016	0.038
422	-0.014	0.004	-0.036	-0.039
431	-0.019	-0.018	-0.031	-0.060
510	-0.016	-0.022	-0.047	-0.057
521	0.015	0.016	0.049	0.052
440	0.029	0.029	0.091	0.153
433	-0.011	-0.009	-0.007	-0.035
530	-0.009	-0.015	-0.031	-0.032
600	-0.025	-0.007	-0.005	0.025
442	0.014	0.013	0.036	0.037

Table 4. Joint Population of 110-200 Shells for Molybdenum Atoms in the Computer Model for Random Ni<sub>4</sub>Mo.

		Number Molybdenum Atoms in (200) Shell						
		0	1	2	3	4	5	6
Number Molybdenum Atoms in (110) Shell	0	38	40	23	9	2	0	0
	1	76	120	87	37	5	1	0
	2	109	179	112	23	11	0	0
	3	125	141	109	26	3	0	0
	4	60	97	54	12	3	0	0
	5	15	32	17	7	0	0	0
	6	7	6	5	2	0	0	0
	7	1	4	0	0	0	0	0

Table 5. Joint Population of 110-200 Shells for Molybdenum Atoms  
in the Computer Model Generated for As-Quenched  $\text{Ni}_4\text{Mo}$ .

		Number Molybdenum Atoms in 200 Shell						
		0	1	2	3	4	5	6
Number Molybdenum Atoms in (110) Shell	0	86	245	279	68	2	0	0
	1	225	374	230	3	0	0	0
	2	76	10	0	0	0	0	0
	3	0	0	0	0	0	0	0
	4	0	0	0	0	0	0	0
	5	0	0	0	0	0	0	0
	6	0	0	0	0	0	0	0

molybdenum atom was examined using a criteria based on the long-range ordered structure; i.e., no molybdenum-molybdenum first neighbors and only one Mo-Mo second nearest neighbors. Generally a criterion based on the first and second shells is sufficient to isolate the regions, but as will be seen on examining Figures 8 and 9, this is not sufficient for  $\text{Ni}_4\text{Mo}$ . The third shell has to be considered before a structure of the clusters can be established. Figures 8 and 9 show five consecutive (100) planes of the computer model for the as-quenched and 5 minutes ordered sample. The symbol 1 represents molybdenum and 0 the nickel atoms. Each plane contains 200 atoms of the total 4000 atoms in the model. The criterion used to mark out the areas was using a Mo atom as the origin, no Mo atoms in the first shell, one or more in the second shell and six or more in the third shell. This criteria closely approximates the model developed by Spruiell (3). The boundary lines drawn show small areas in which the criterion was satisfied. The areas are four to six atoms diameter in size, or approximately 15 to 20 Å. This is indeed the size of the microdomains that have claimed to exist in this alloy (3,9). This size of the domains does not change much on ordering for 5 minutes at 650°C, but the order is more complete as seen in Figure 9. An attempt was made to see if the composition fluctuations mentioned by Okamoto (5) could be observed in these computer maps. This failed since the areas mentioned are so small that a sufficient number of (420) planes were not found.

Streaks of intensity along the [100] directions are observed at the peak positions of the diffuse intensity distributions shown in



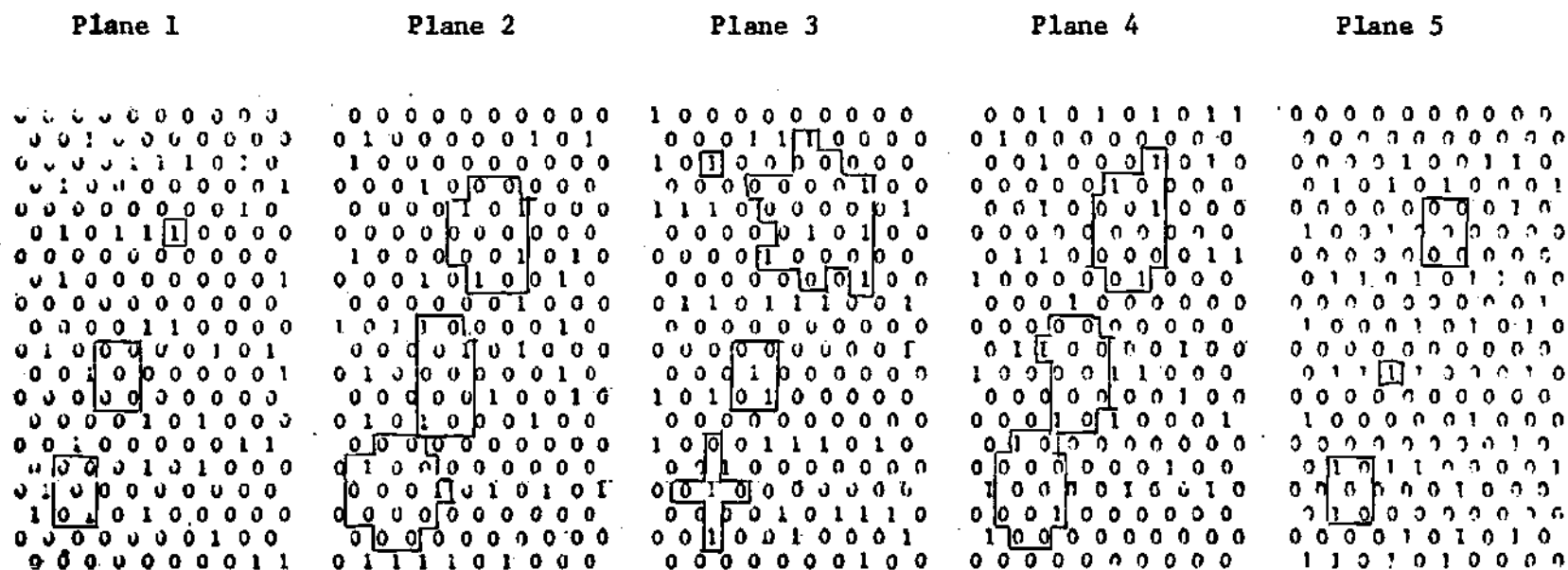


Figure 8. Atomic Arrangements of Computer Generated Model for As-Quenched Ni<sub>4</sub>Mo. (Plane 1 stacks on top of 2, 2 on top of 3 and so on).

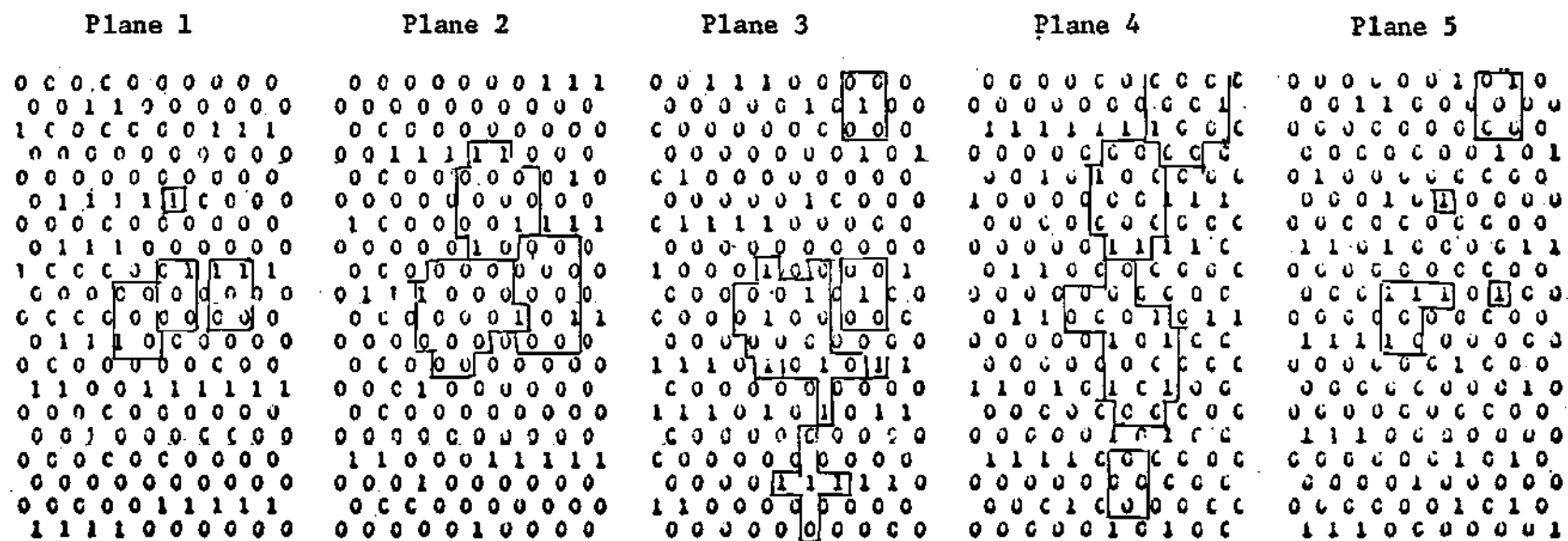


Figure 9. Atomic Arrangements of Computer Generated Model for Alloy Aged for 5 Minutes at 650°C.

Figures 2 and 3. The streaks get more prominent on ordering at 650°C and are accompanied by a large rise in the value of  $\alpha_{200}$ , from -0.010 to 0.112 (Table 2). This feature was reproduced in the short-range coefficients obtained from the simulated model (Table 3). Thus it is to be expected that the computer maps would show this feature and indeed they do. Figure 10, for as-quenched alloy shows that the atomic configuration consists of rods on (200) planes lying in  $\langle 100 \rangle$  directions. About 55 percent of the molybdenum atoms in the model are in the rods. As the alloy orders the rods get longer as seen in Figure 11 for the 5 minutes ordered case. Here about 63 percent of the molybdenum atoms are in the rods configuration. The morphology described here, although never before discussed for  $\text{Ni}_4\text{Mo}$ , has been suggested for nickel-10 atomic percent tungsten alloy (26). The nickel-tungsten system is very similar to the nickel-molybdenum system and  $\text{Ni}_4\text{W}$  is structurally the same as  $\text{Ni}_4\text{Mo}$  (28). Okamoto shows photographs of microdomains in  $\text{Ni}_4\text{Mo}$  ordered for 10 minutes at 750°C and claims that the microdomains are equiaxed and have a size distribution of 20 to 100 Å. However, close examination of Figure 10b in reference 5 shows those microdomains as small rods. Okamoto also claims that "there is a slight tendency for the domains of a particular variant to align themselves in rows was observed with longer ageing times but neither with sufficient frequency nor with sufficient directional uniqueness to establish any definite relationship with a diffraction effect." The field-ion (5) micrographs also show clusters of molybdenum atom in a rod-like fashion. We conclude that the as-quenched structure of  $\text{Ni}_4\text{Mo}$  has rod-like clusters of molybdenum atoms which satisfy the primary characteristic of  $\text{Ni}_4\text{Mo}$ , in that there are no Mo-Mo first

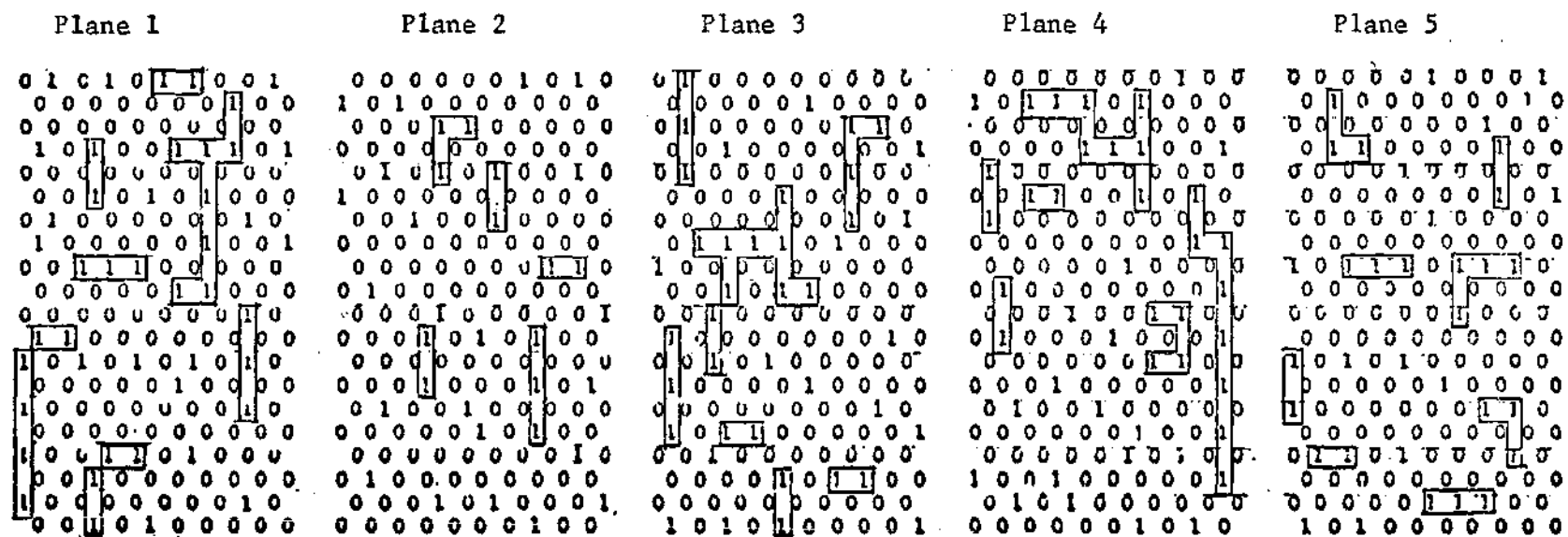


Figure 10. Atomic Arrangements of Computer Generated Model for As-Quenched  $\text{Ni}_4\text{Mo}$  Showing Rodlike Morphology.



Table 6. Three Dimensional First Order Size Effect Coefficients for  $\text{Ni}_4\text{Mo}$  Quenched from  $1000^\circ\text{C}$ .

LMN	$\gamma_{lmn}^l$	$\gamma_{lmn}^m$	$\gamma_{lmn}^n$
000	0.000	0.000	0.000
110	0.000	0.000	0.000
200	0.115	0.000	0.000
211	0.010	0.000	0.000
220	0.112	0.112	0.000
310	0.000	0.000	0.000
222	0.076	0.076	0.076
321	0.000	0.028	0.000
400	0.029	0.000	0.000
330	0.000	0.000	0.000
411	0.092	0.000	0.000
420	0.063	0.042	0.000
332	0.000	0.000	0.037
422	0.057	0.037	0.037
431	0.071	0.000	0.000
440	0.045	0.045	0.000
433	0.051	0.000	0.000
442	0.045	0.045	0.012
444	0.026	0.026	0.026

Table 7. Three Dimensional First Order Size Effect Coefficients for  $Ni_4Mo$ , Quenched From  $1000^{\circ}C$  and Ordered 5 Minutes at  $650^{\circ}C$ .

LMN	$\gamma_{lmn}^l$	$\gamma_{lmn}^m$	$\gamma_{lmn}^n$
000	0.000	0.000	0.000
110	0.000	0.000	0.000
200	0.092	0.000	0.000
211	-0.001	0.000	0.000
220	0.084	0.084	0.000
310	0.000	0.000	0.000
222	0.038	0.038	0.038
321	0.000	0.019	0.000
400	-0.002	0.000	0.000
330	0.000	0.000	0.000
411	0.048	0.000	0.000
420	0.052	0.029	0.000
332	0.000	0.000	0.020
422	0.037	0.014	0.014
431	0.032	0.000	0.000
440	0.025	0.025	0.000
433	0.023	0.000	0.000
442	0.017	0.017	0.009
444	0.019	0.019	0.019

Table 8. Three Dimensional First Order Size Effect Coefficients for  $\text{Ni}_4\text{Mo}$ , Quenched from  $1000^\circ\text{C}$  and Ordered 10 Minutes at  $650^\circ\text{C}$ .

LMN	$\gamma_{lmn}^l$	$\gamma_{lmn}^m$	$\gamma_{lmn}^n$
000	0.000	0.000	0.000
110	0.000	0.000	0.000
200	0.005	0.000	0.000
211	-0.015	0.000	0.000
220	0.083	0.083	0.000
310	0.000	0.000	0.000
222	0.066	0.066	0.066
321	0.000	0.016	0.000
400	-0.116	0.000	0.000
330	0.000	0.000	0.000
411	0.036	0.000	0.000
420	0.051	-0.010	0.000
332	0.000	0.000	0.015
422	0.082	0.005	0.005
431	0.023	0.000	0.000
440	-0.015	-0.015	0.000
433	0.012	0.000	0.000
442	0.006	0.006	-0.014
444	0.003	0.003	0.003



nearest neighbors. This morphology also explains the unusual rise in  $\alpha_{200}$  and the [100] streaking observed in the diffuse scattering maps.

## CHAPTER V

### CONCLUSIONS AND RECOMMENDATIONS

#### Conclusions

The three-dimensional diffuse scattering measurements have been analyzed for the as-quenched  $\text{Ni}_4\text{Mo}$  and show that the structure in the quenched state has tiny rodlike regions. These rods:

- i) satisfy the primary requirement of the LRO structure in that there are no molybdenum-molybdenum neighbors in the first shell;
- ii) grow on ordering;
- iii) satisfies the measured alpha parameters and explain the streaks of intensity observed in the measured diffuse scattering.

#### Recommendations

The local order coefficients obtained from this study can be used for the following calculations and modeling which will aid in a general understanding of solid solutions:

- (i) The alphas can be used to test the validity of the quasi-chemical approach to solid solutions. The quasi-chemical theory maintains that the energy of a solution is given by the sum of constant pairwise interaction energies between the various neighbors and that volume and vibrational changes accompanying the formation of the alloy from its components can be neglected. We may use the short-range order coefficients to extract the interaction energies from a set of simultaneous equations, provided sufficient coefficients are available.

Using these interaction energies the validity of Clapp and Moss's (11) theory, i.e., that the disordered state above  $T_c$  is best described by a "liquid-like" structure or a statistical model of  $\mathbb{R}O$ , can be checked.

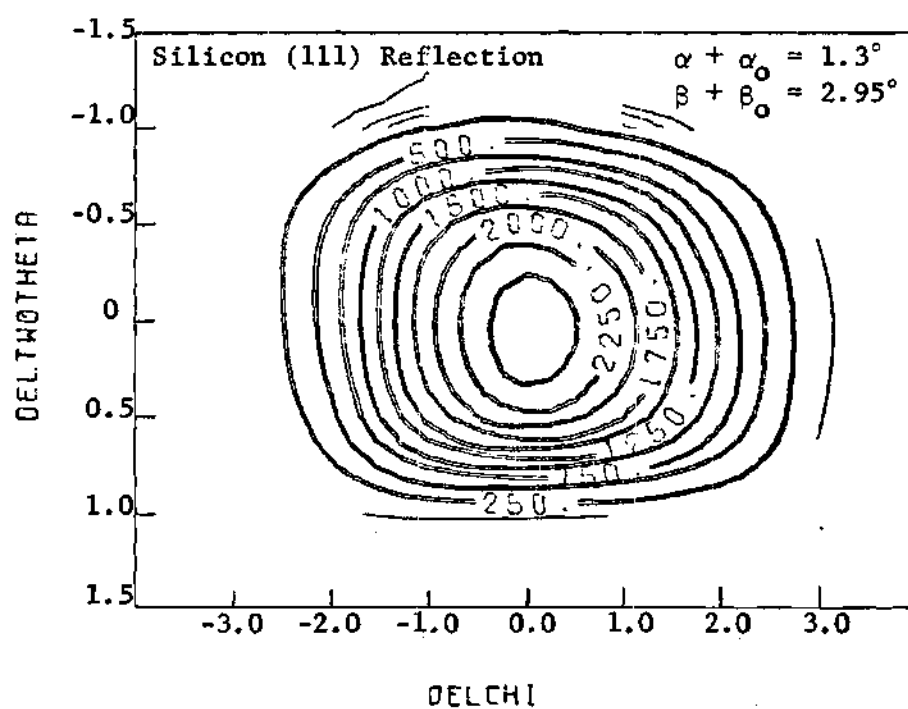
(ii) The short-range order coefficients can be used to calculate thermodynamics data, e.g.,  $\Delta H_{\text{configurational}} = NX \sum_A X_B \sum_i C_i \alpha_i V_i$  and the calculated value be compared with that obtained from specific heat data.

(iii) The alphas can be used to predict configurational changes, and therefore the strength, of  $Ni_4Mo$  due to deformation.

(iv) Finally, an analysis of the static displacement coefficients determined from the diffuse scattering experiments can be made in order to clarify the elastic properties of  $Ni_4Mo$ .

## APPENDIX A

## DIFFUSE INTENSITY MAPS AND TABLES



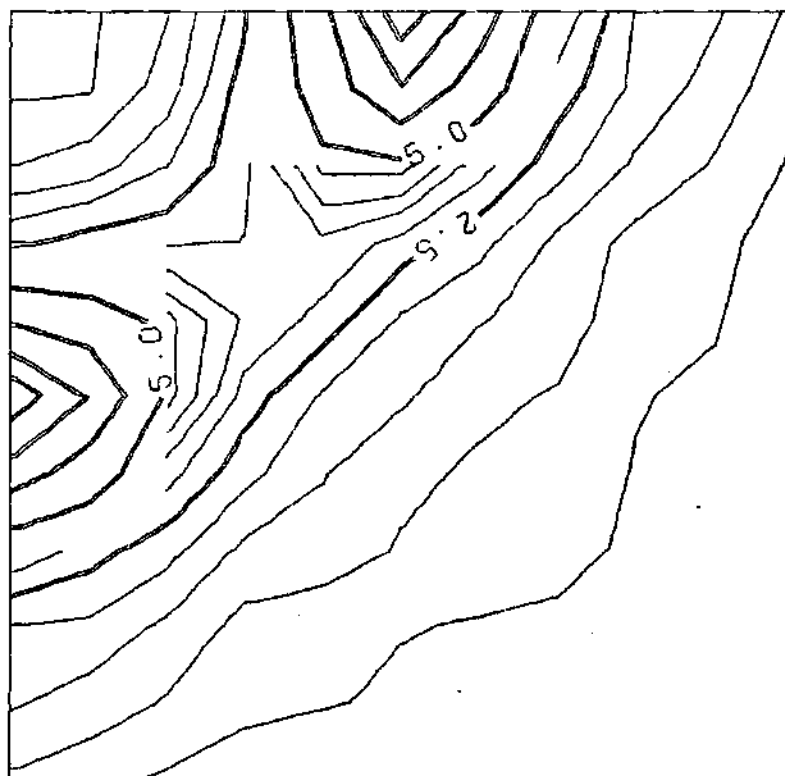
DIRECT BEAM INTENSITY CONTOURS

OFF DOUBLY BENT GRAPHITE

MONOCHROMATOR

## SR0 INTENSITY

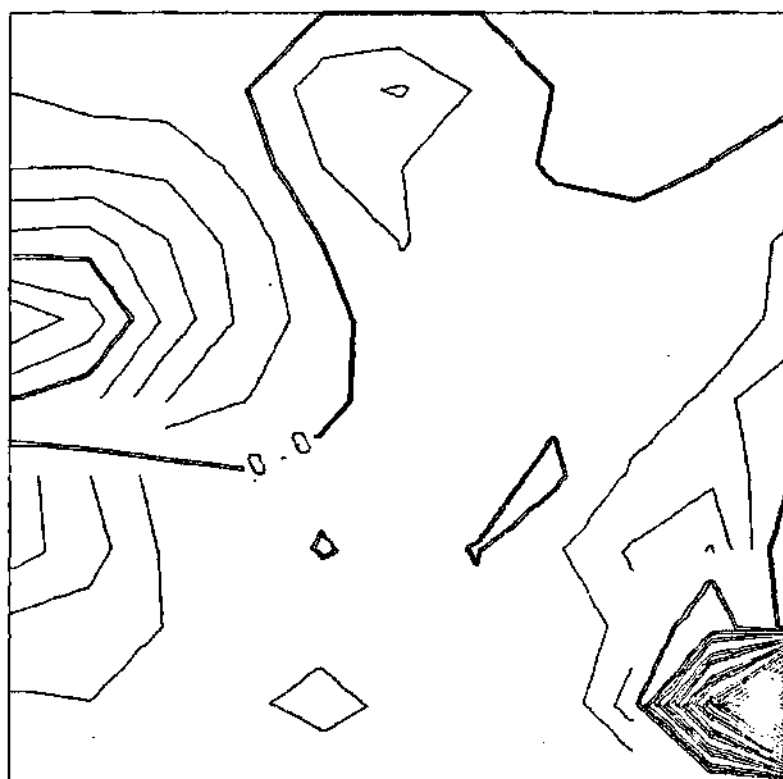
H1.H2=1.0.0.5



H1.H2=0.5.0.0

H1.H2=1.0.0.0

## SIZE EFFECT INTENSITY

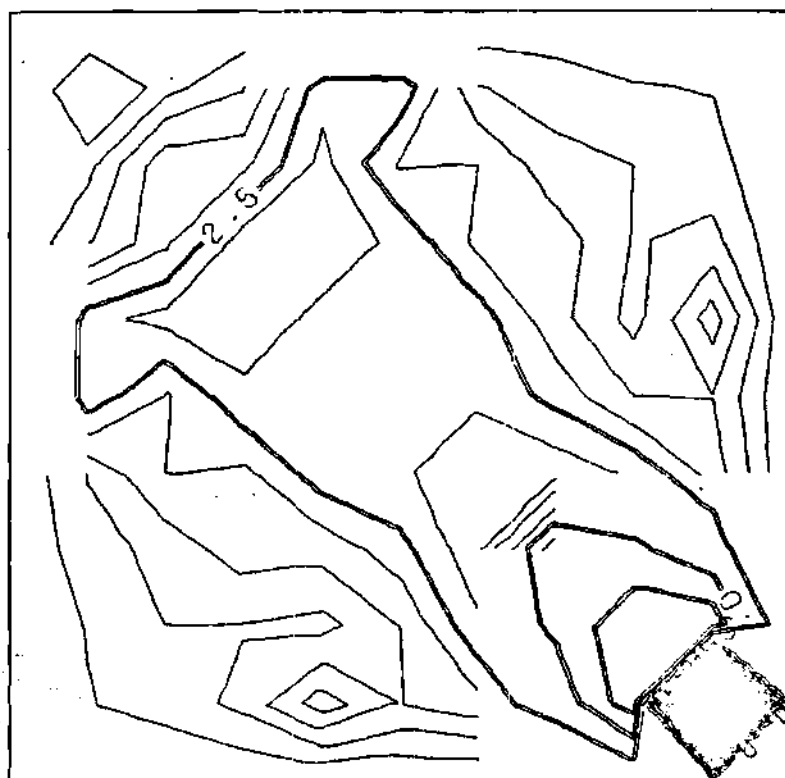
 $H1, H2 = 1.0, 0.5$  $H1, H2 = 0.5, 0.0$  $H1, H2 = 1.0, 0.0$

## DEL SQUARE INTENSITY

 $H_1, H_2 = 1.0, 0.5$  $H_1, H_2 = 0.5, 0.0$  $H_1, H_2 = 1.0, 0.0$



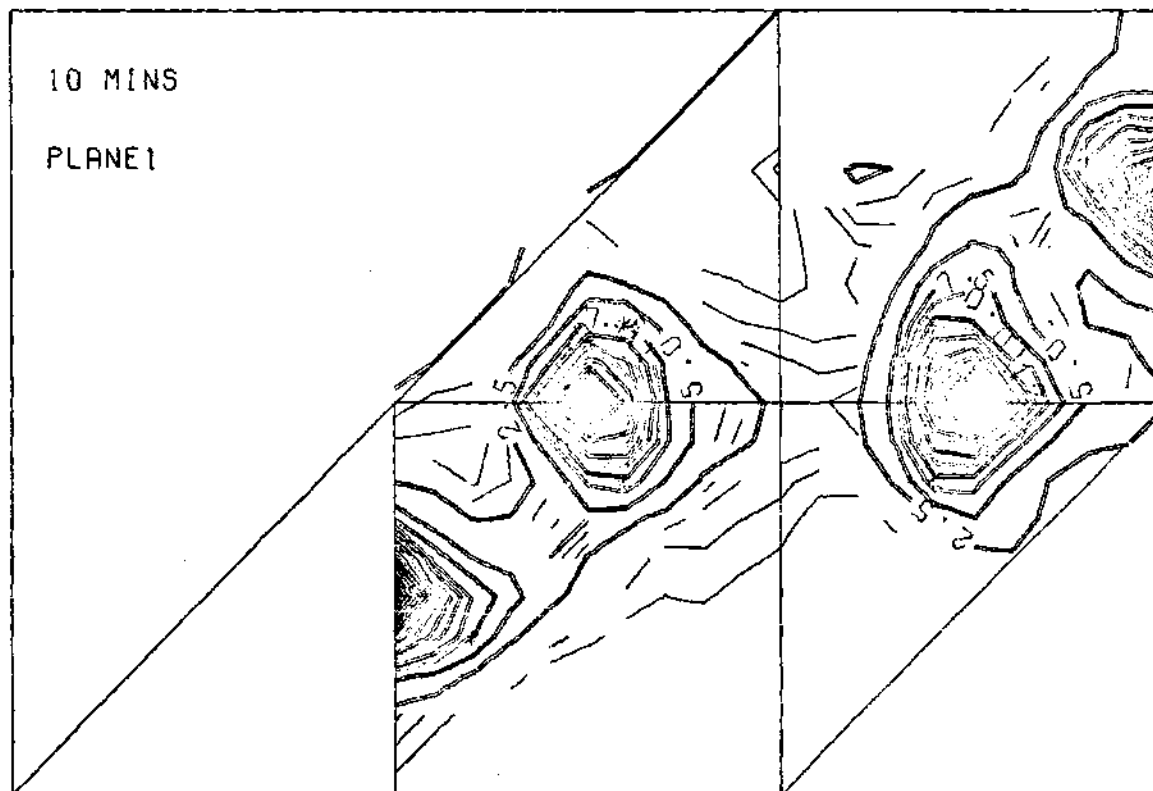
## DEL CROSS INTENSITY

 $H_1.H_2=1.0.0.5$  $H_1.H_2=0.5.0.0$  $H_1.H_2=1.0.0.0$

H1.H2=1.0.1.0

10 MINS

PLANE1



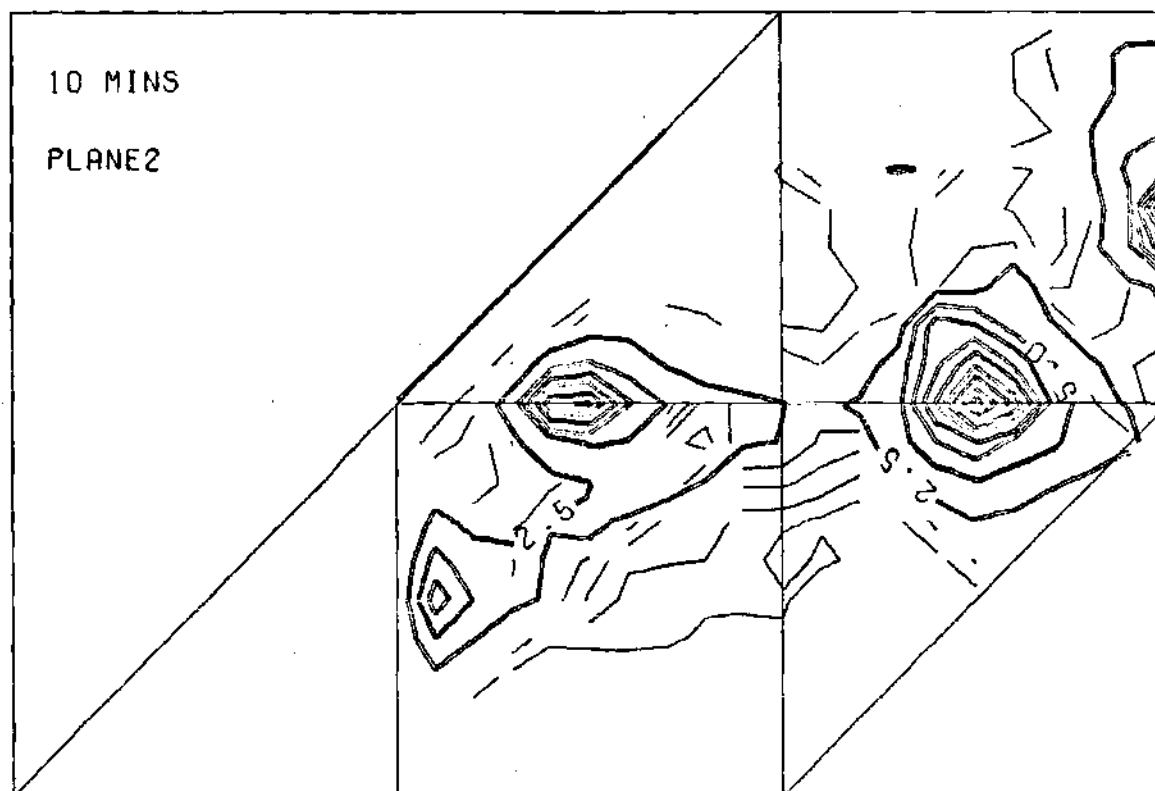
H1.H2=0.0.0.0

H1.H2=1.0.0.0

H1.H2=1.0.1.0

10 MINS

PLANE2



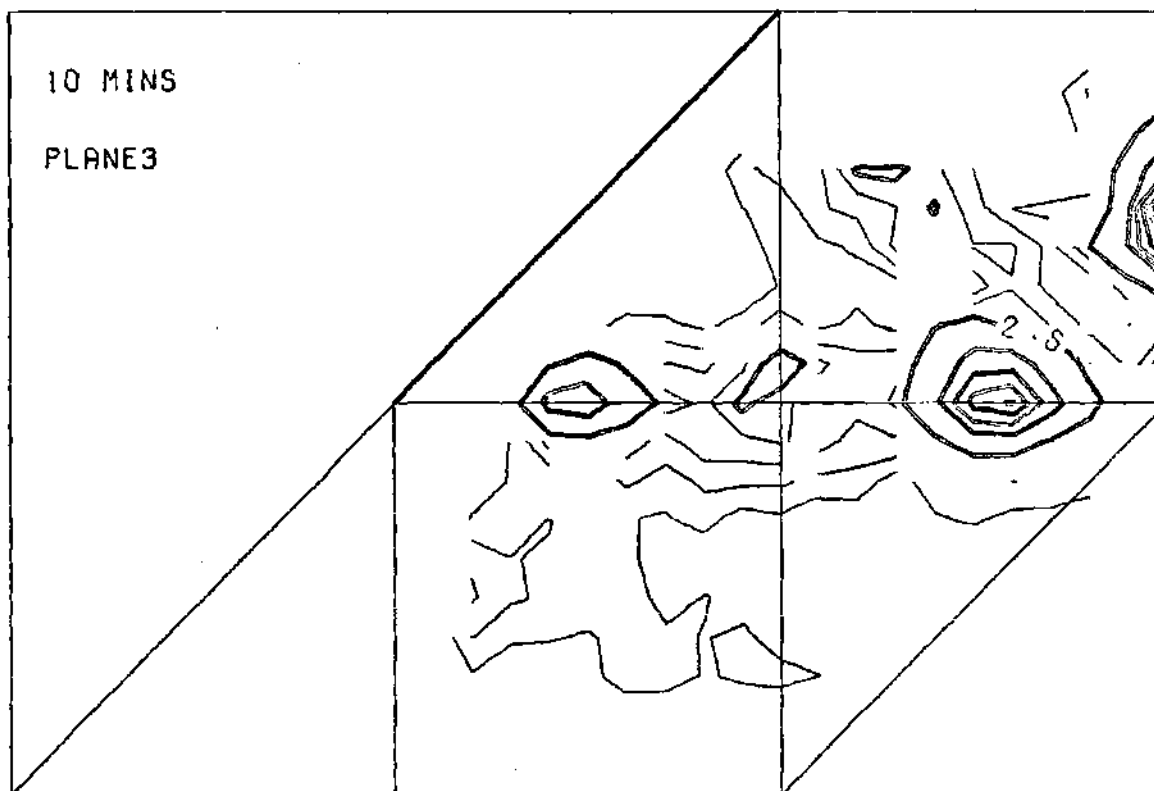
H1.H2=0.0.0.0

H1.H2=1.0.0.0

H1.H2=1.0.1.0

10 MINS

PLANE3



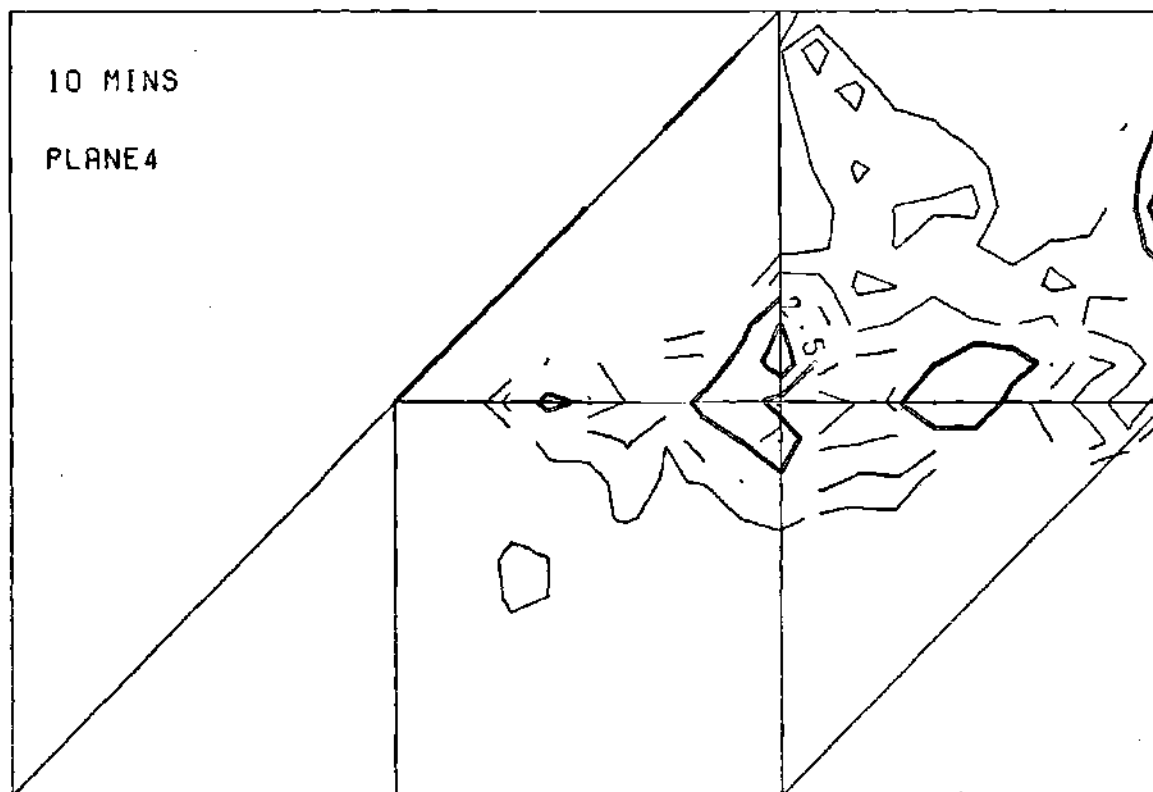
H1.H2=0.0.0.0

H1.H2=1.0.0.0

H1,H2=1.0.1.0

10 MINS

PLANE4



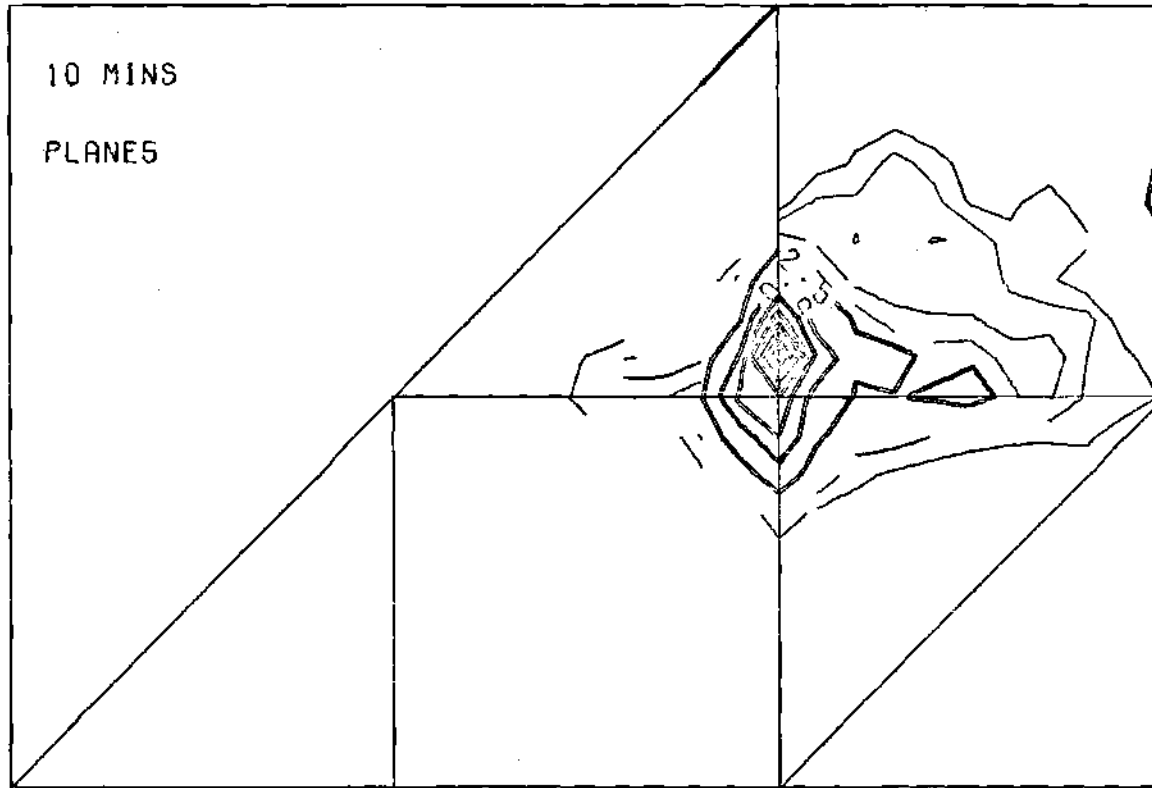
H1,H2=0.0.0.0

H1,H2=1.0.0.0

H1,H2=1.0,1.0

10 MINS

PLANES



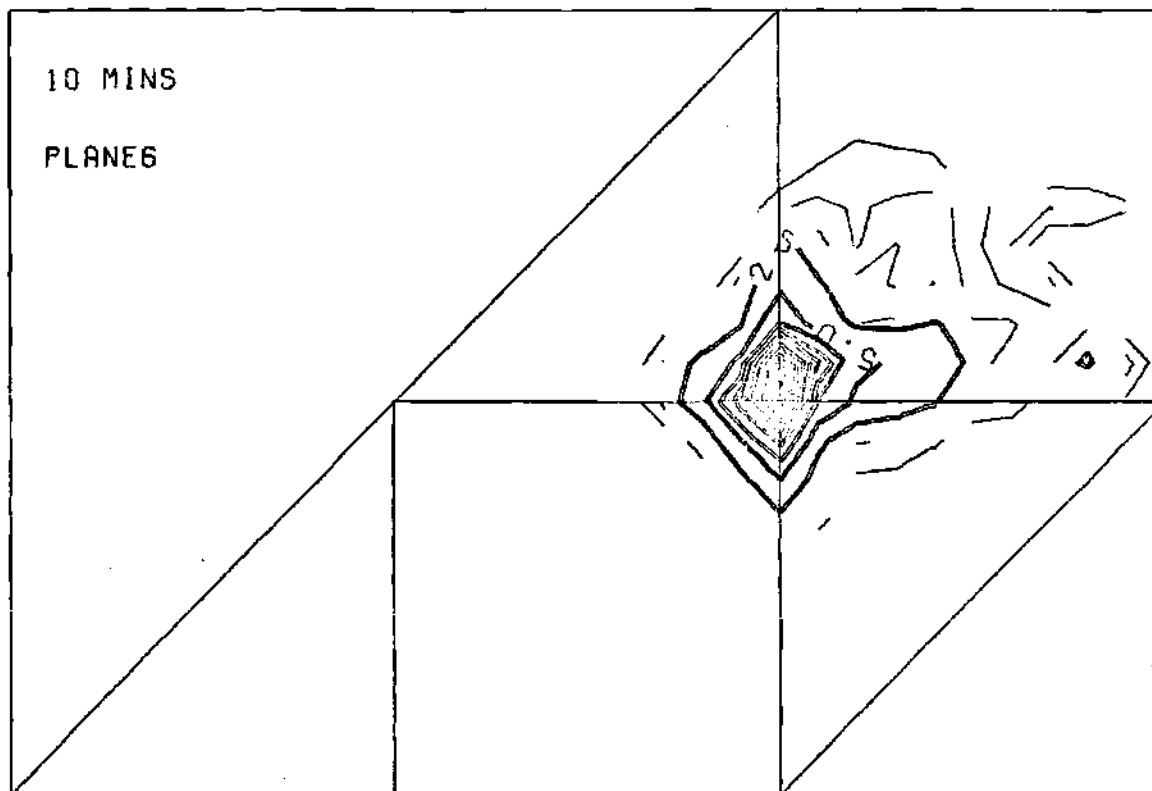
H1,H2=0.0,0.0

H1,H2=1.0,0.0

H1.H2=1.0.1.0

10 MINS

PLANES



H1.H2=0.0.0.0

H1.H2=1.0.0.0

Three Dimensional Delsquare Coefficients for  $\text{Ni}_4\text{Mo}$  Quenched from  $1000^\circ\text{C}$ .

LMN	$\langle \delta^2 \rangle_{lmn}^1$	$\langle \delta^2 \rangle_{lmn}^m$	$\langle \delta^2 \rangle_{lmn}^n$
000	0.374	0.374	0.374
110	0.890	0.890	1.008
200	0.615	0.782	0.782
211	0.830	0.803	0.803
220	0.745	0.745	0.898
310	0.730	0.716	0.763
222	0.713	0.713	0.713
321	0.589	0.663	0.705
400	0.488	0.653	0.653
330	0.549	0.549	0.630
411	0.468	0.625	0.625
420	0.487	0.560	0.575
332	0.505	0.505	0.508
422	0.431	0.485	0.485
431	0.395	0.460	0.459
440	0.320	0.320	0.392
433	0.299	0.323	0.323
442	0.288	0.288	0.304
444	0.165	0.165	0.165



Three Dimensional Delsquare Coefficients for Ni<sub>4</sub>Mo Quenched from 1000°C,  
and Ordered 5 Minutes at 650°C.

LMN	$\langle \delta^2 \rangle_{lmn}^1$	$\langle \delta^2 \rangle_{lmn}^m$	$\langle \delta^2 \rangle_{lmn}^n$
000	-0.291	-0.291	-0.291
110	-0.045	-0.045	-0.040
200	-0.231	-0.073	-0.073
211	0.015	-0.038	-0.038
220	-0.032	-0.032	-0.017
310	0.080	-0.041	-0.019
222	0.058	0.058	0.058
321	-0.004	0.000	0.016
400	0.026	-0.009	-0.009
330	0.024	0.024	0.010
411	0.062	-0.001	-0.001
420	0.072	-0.014	-0.038
332	0.029	0.029	-0.005
422	0.080	-0.007	-0.007
431	0.064	0.037	-0.005
440	0.029	0.029	0.012
433	0.054	0.020	0.020
442	0.033	0.033	0.023
444	0.022	0.022	0.022

Three Dimensional Delsquare Coefficients for Ni<sub>4</sub>Mo Quenched from 1000°C,  
and Ordered 10 Minutes at 650°C.

LMN	$\langle \delta^2 \rangle_{lmn}^1$	$\langle \delta^2 \rangle_{lmn}^m$	$\langle \delta^2 \rangle_{lmn}^n$
000	-0.504	-0.504	-0.504
110	-0.038	-0.038	0.095
200	-0.182	-0.085	-0.085
211	-0.023	-0.016	-0.016
220	0.036	0.036	-0.066
310	0.113	-0.039	0.038
222	0.110	0.110	0.110
321	-0.006	-0.014	0.004
400	-0.002	-0.023	-0.023
330	0.051	0.051	0.065
411	0.112	0.036	0.036
420	0.077	0.014	-0.040
332	0.046	0.046	0.011
422	0.088	0.014	0.014
431	0.097	0.050	0.017
440	0.034	0.034	0.012
433	0.067	0.022	0.022
442	0.039	0.039	0.027
444	0.028	0.028	0.028

Three Dimensional Delcross Coefficients for  $\text{Ni}_4\text{Mo}$  Quenched from  $1000^\circ\text{C}$

LMN	$\langle \delta \rangle_{lmn}^2$	$\langle \delta \rangle_{lmn}^2$	$\langle \delta \rangle_{lmn}^2$
000	0.000	0.000	0.000
110	-0.373	0.000	0.000
200	0.000	0.000	0.000
211	0.000	-0.094	0.000
220	-0.222	0.000	0.000
310	-0.161	0.000	0.000
222	-0.176	-0.176	-0.176
321	0.000	0.000	-0.115
400	0.000	0.000	0.000
330	-0.297	0.000	0.000
411	0.000	-0.024	0.000
420	-0.224	0.000	0.000
332	-0.261	0.000	0.000
422	-0.239	-0.144	-0.239
431	0.000	-0.099	0.000
440	-0.378	0.000	0.000
433	0.000	-0.254	0.000
442	0.371	-0.215	-0.215
444	-0.341	-0.341	-0.341

Three Dimensional Delcross Coefficients for Ni<sub>4</sub>Mo Quenched from 1000°C  
and Ordered 5 Minutes at 650°C.

LMN	$\langle \delta \rangle_{lmn}^2$	$\langle \delta \rangle_{lmn}^2$	$\langle \delta \rangle_{lmn}^2$
000	0.000	0.000	0.000
110	-0.302	0.000	0.000
200	0.000	0.000	0.000
211	0.000	-0.064	0.000
220	-0.045	0.000	0.000
310	-0.036	0.000	0.000
222	-0.031	-0.031	-0.031
321	0.000	0.000	-0.009
400	0.000	0.000	0.000
330	0.003	0.000	0.000
411	0.000	-0.005	0.000
420	0.015	0.000	0.000
332	0.029	0.000	0.000
422	-0.003	0.001	-0.003
431	0.000	-0.004	0.000
440	0.019	0.000	0.000
433	0.000	0.022	0.000
442	0.005	0.011	0.011
444	0.020	0.020	0.020

Three Dimensional Debye Coefficients for Ni<sub>4</sub>Mo Quenched from 1000°C  
and Ordered 10 Minutes at 650°C.

LMN	$\langle \delta^2 \rangle_{lmn}^{lm}$	$\langle \delta^2 \rangle_{lmn}^{mn}$	$\langle \delta^2 \rangle_{lmn}^{nl}$
000	0.000	0.000	0.000
110	-0.359	0.000	0.000
200	0.000	0.000	0.000
211	0.000	-0.061	0.000
220	-0.077	0.000	0.000
310	-0.065	0.000	0.000
222	-0.038	-0.038	-0.038
321	0.000	0.000	-0.024
400	0.000	0.000	0.000
330	-0.007	0.000	0.000
411	0.000	-0.011	0.000
420	-0.014	0.000	0.000
332	0.024	0.000	0.000
422	-0.020	0.013	-0.020
431	0.000	-0.013	0.000
440	-0.021	0.000	0.000
433	0.000	0.001	0.000
442	0.026	0.008	0.008
444	0.011	0.011	0.011

## APPENDIX B

### COMPUTER PROGRAMS

## PROGRAM DIFVOL

THIS PROGRAM CALCULATES THE DIFFRACTION COORDINATES  
FOR A SQUARE GRID IN THE FCC 3D VOLUME FOR MAKING  
DIFFUSE SCATTERING MEASUREMENTS.  
OUTPUT DTEX INSTRUCTIONS.

```

10 FORMAT ( 1HN,3I3,5H/1026,I5,5HT1026,I5,10H*102600000,
15H=2026,I5,5H=2006,I5 )
20 FORMAT (1HK, 35HNUMBER OF POINTS IN THIS ELEMENT IS, I5 )
40 FORMAT(5F10.5)
41 FORMAT(1H1,20X,3HN1=,F9.6,3HN2=,F9.6,3HN3=,F9.6///
120X,6HAZERO=,F9.6///20X,7HLAMBDA=,F9.6 )
100 FORMAT(1H1, 50X,5HPLANE,I5)
120 FORMAT ( 1H0, 50X, 4HLINE, I5 )
150 FORMAT ( 40HV, 1 1 1/102601252T102600000*102600000,
120H=202605222=200605222 )
    DIMENSION TOTHTA(41,41) , CHI(41,41) , PHI(41,41) ,
    1B(41,41) , C(41,41) , ITOTHA(41,41) , ICHI(41,41) ,
    2A(41,41) , IPHI(41,41)
    REAL LAMBDA,N1,N2,N3
    READ(5,40) N1,N2,N3,AZERO,LAMBDA
    WRITE(6,41) N1,N2,N3,AZERO,LAMBDA
    H100=0.50
    H200=0.00
    H300=0.0
    DLTAH1=0.05
    DLTAH2=0.05
    DLTAH3=0.05
    Z=0.0174532925
16 DO 1000 K=1,6
    1 N=0
    M=0
    WRITE(6,100) K
    WRITE ( 1,150)
    RK=K-1
    H3 = H300 + (RK*DLTAH3 )
    KK=21
25 KM=K
    DO 2000 J=KM,KK
    WRITE (6,120 ) J
    RJ=J-1
    H2 = H200 + (RJ*DLTAH2 )
    IF ( J .GE. 11 ) GO TO 75
    IF ( J .GT. 12-K ) GO TO 55
    IK=K
    KKK=10+J
    GO TO 65
55 IK = 12-J

```

```

      KKK = 10+J
      GO TO 65
75  IK = J - 10
      IF ( J .GE. 10+K .AND. J .LE. 22-K ) GO TO 85
      KKK= 22-IK
      GO TO 65
85  KKK= 21
65  DO 3000 I=IK,KKK
      N=N+1
      M=M+1
      RI=I-1
      H1 = H100 + (RI*DLTAH1 )
      F = (LAMBDA/AZERO ) * ( SQRT( H1**2 + H2**2 + H3**2 ) )
      TOTHTA(I,J)=(2.0/Z)* ASIN(F)
      C(I,J) = TOTHTA(I,J) * 100.0
      ITOTHA(I,J) = C(I,J)
      FF = (H1*N1 + H2*N2 + H3*N3 )/((SQRT(H1**2 + H2**2 +
1H3**2 ))*(SQRT(N1**2 + N2**2 + N3**2 )))
      CHI(I,J)=(1.0/Z)* ACOS(FF)
      A(I,J) = CHI(I,J) * 100.0
      ICHI(I,J) = A(I,J)
      FFFF = Z*CHI(I,J)
      FFF = ( H3*N1 - H1*N3 ) /((SQRT(N1**2 + N3**2)) *
1(SQRT( H1**2 + H2**2 + H3**2)) * SIN(FFFF) )
      PHI(I,J) = (1.0/Z) * ASIN(FFF)
      GO TO 750
750 B(I,J) = PHI(I,J) * 100.0
      IPHI(I,J) = B(I,J)
      COS 1 = N1/(( N1**2 + N2**2 ) **0.5 )
      COS 2 = H1/(( H1**2 + H2**2 ) **0.5 )
      IF ( COS 2 .GE. COS 1 ) GO TO 1500
      ICHI(I,J) = 36000 - ICHI(I,J)
1500 WRITE ( 1,10 ) I,J,K,ICHI(I,J) , IPHI(I,J), ITOTHA(I,J),
1ITOTHA(I,J)
      IF ( M .LT. 50 ) GO TO 3000
      WRITE (1,150 )
      M=0
3000 CONTINUE
2000 CONTINUE
      WRITE (6,20) N
1000 CONTINUE
      CALL EXIT
      END

```



## PROGRAM INTCOR

```

THIS PROGRAM CORRECTS THE TOTAL DIFFUSE SCATTERED
INTENSITY FOR POLARISATION, RESONANCE AND
COMPTON INTENSITY AND FINALLY DIVIDES BY THE LAUE
MONOTONIC INTENSITY FOR THE FCC 3D VOLUME OF SPARKS.
MODIFIED FROM THE 2D TO 3D VERSION BY B.CHAKRAVARTI.
REAL MWP, MAS, MAPL, IOVRMP, LMONO(21,21), IPOLY,
1INTCOR( 21,21), IMEAS(21,21), INTNOR(21,21), IS(21,21)
  DIMENSION FNI(105), FMO(105), COMPNI(105), COMPMO(105),
1 TOTHTA(21,21), INT(21,21), C(21,21), COMP(21,21),
2POLF(21,21), BREMST(21,21)
1 FORMAT(8F10.5)
2 FORMAT (16F5.2)
3 FORMAT(16I5)
5 FORMAT (1H1,50X,5HPLANE,I5 )
4 FORMAT ( 54X,I6,14X, I6 )
6 FORMAT ( 1H0, 50X, 4HLINE, I5 )
8 FORMAT ( 45X,F5.2,4X,I6,14X,I6 )
10 FORMAT(1H, 3I3,2X,F5.2,3X,F5.2,2X,F5.2,2(2X,F7.2),2X,F7.3,
11X,F7.3,2X,F5.2,1X,F5.2 )
12 FORMAT ( 1HK, 35HNUMBER OF POINTS IN THIS ELEMENT IS, I5 )
25 FORMAT(1H0,2X,1H1,2X,1HJ,2X,1HK,1X,7HTO TETA, 2X,5HFOFNI,
12X,5HFOFMO,2X,7HRAW INT,2X,7HNORMINT, 2X, 7HCOE INT,1X,
27HINT NOR,2X,5HLMONO,1X,5HCMINT )
45 FORMAT(1H1,10X,3HFNI,7X,3HFMO,7X,6HCOMPNI,4X,6HCOMPMO )
41 FORMAT (1H, 9X,F5.2,4X,F5.2,7X,F5.2,5X,F5.2 )
Z = 0.0174532925
READ ( 5, 1 )AWS, MWP, MAS, MAPL,IOVRMP, IPOLY, XSUBXA
READ (5,1 ) ANGM, ANGP, BREM
READ (5, 3) ISS, IFI
READ ( 5, 2 ) (FNI(I), I= ISS,IFI )
READ ( 5, 2 ) (FMO(I), I= ISS,IFI )
READ ( 5, 2 ) ( COMPNI(I), I= ISS, IFI )
READ ( 5, 2 ) ( COMPMO(I), I= ISS, IFI )
WRITE(6,45)
WRITE(6,41) ( FNI(I),FMO(I),COMPNI(I),COMPMO(I),
1I=ISS,IFI )
WRITE ( 6, 1 ) AWS, MWP, MAS, MAPL,IOVRMP, IPOLY, XSUBXA
WRITE ( 6, 1 ) ANGM, ANGP, BREM
WRITE ( 6,3 ) ISS, IFI
Y= ( AWS*MAS*IOVRMP ) / ( MWP*MAPL*IPOLY )
COSM = (COS(Z*ANGM))
COSP = ( COS(Z*ANGP))**2
PN = 1.0 + COSM*COSP
WRITE (6,1) Y,COSM, COSP, PN
30 DO 1000 K = 1,6
  N=0
  M=0

```

```

WRITE ( 6, 5 ) K
WRITE ( 6, 25 )
READ(5,4) INORNI, INORCO
INORM = INORNI - INORCO
READ (5,4 ) ICHKNI, ICHKCO
ICKK = ICHKNI - ICHKCO
A=FLOAT(INORM)/FLOAT(ICKK)
WRITE ( 6,1 ) A
KK = 21
KM = K
DO 2000 J = KM, KK
WRITE (6 ,6 ) J
IF ( J .GT. 11 ) GO TO 50
IF ( J .GT. 12-K ) GO TO 40
IK = K
KKK = 10+ J
GO TO 65
40 IK = 12-J
KKK = 10+ J
GO TO 65
50 IK = J- 10
IF ( J .GE. 10+K .AND. J .LE. 22-K ) GO TO 60
KKK = 22- IK
GO TO 65
60 KKK=21
65 I=IK
70 IF ( I .GT. KKK ) GO TO 3000
N=N+1
M=M+1
IF ( M .LT. 51 ) GO TO 85
READ(5,4) ICHKNI, ICHKCO
ICKK = ICHKNI - ICHKCO
A=FLOAT(INORM)/FLOAT(ICKK)
WRITE ( 6,1 ) A
M=0
GO TO 70
85 READ(5,8) TOTHTR, INTNI, INTO
TOTHTA(I,J) = TOTHTR
III= TOTHTA(I,J)
C(I,J) = III
DELT = TOTHTA(I,J) - C(I,J)
INT(I,J) = INTNI - INTO
IMEAS(I,J)= FLOAT(INT(I,J))/60.0
C POLARISATION FACTOR
COSS = ( COS(2*TOTHTA(I,J)))**2
POLF(I,J) = PN/(1.0 + COSM*COSS)
C RESONANCE CORRECTIONS
BREMST(I,J) = BREM / (1.0+COSM*COSS)
C COMPTON INTENSITY
COMPL0 =XSUBXA*COMPM0(III) + (1.0-XSUBXA)*COMPM1(III)
COMPHI =XSUBXA*COMPM0(III+1) + (1.0-XSUBXA)*COMPM1(III+1)

```

```

      COMP(I,J) = COMPL0 + DELT*(COMPHI-COMPL0 )
LAUE MONOTONIC INTENSITY
      FOFNI = FNI(III) + DELT*(FNI(III+1) -FNI(III))
      FOFMO = FMO(III) + DELT*(FMO(III+1) -FMO(III))
      LMONO(I,J) = XSUBXA*(1.0-XSUBXA)*((FOFMO-FOFNI)**2)
CORRECTED INTENSITY
      INTCOR(I,J) = ( (Y*POLF(I,J)*IMEAS(I,J)) - (COMP(I,J)+
1BREMST(I,J)) ) / LMONO(I,J)
      INTNOR(I,J) = ( (Y*POLF(I,J)*IS(I,J)) - (COMP(I,J)+
1BREMST(I,J)) ) / LMONO(I,J)
      WRITE(6,10) I,J,K, 10HTA(I,J), FOFNI,FOFMO,
1IMEAS(I,J), IS(I,J), INTCOR(I,J), INTNOR(I,J),
2LMONO(I,J), COMP(I,J)
      I = I+1
      GO TO 70
3000 CONTINUE
2000 CONTINUE
      WRITE(6,12) N
1000 CONTINUE
      CALL EXIT
      END

```

## PROGRAM SEPRIT

THIS PROGRAM SEPARATES THE MEASURED DIFFUSE INTENSITY INTO THE FOUR COMPONENTS BY THE QUADRATIC SEPARATION METHOD FOR THE THREE DIMENSIONAL CASE.

```

17 FORMAT(10X,I5 )
690 FORMAT(1X,2I3,3X,F7.3)
700 FORMAT(1H1,59X,15HIDIFFUSE(H1,H2)/)
710 FORMAT(1H1,61X,11HT1H2(H1,H2)/)
720 FORMAT(1H1,61X,11HT2H2(H1,H2)/)
730 FORMAT(1H1,61X,11HT1H1(H1,H2)/)
740 FORMAT(1H1,62X,9HT4(H1,H2)/)
750 FORMAT(16I5)
760 FORMAT(1H ,16I5)
770 FORMAT ( 20X, F7.3 )
780 FORMAT(1X,2I3,41X,F7.3,4X,F5.2 )
800 FORMAT(1HK,20H* (H1,H2)=(0.0,-1.5),90X,
120H(H1,H2)=(1.5,-1.5) *)
810 FORMAT(1HK,19H* (H1,H2)=(0.0,1.5),92X,
119H(H1,H2)=(1.5,1.5) *)
820 FORMAT(1HK,20H* (H1,H2)=(0.5,-0.5),90X,
120H(H1,H2)=(1.5,-0.5) *)
830 FORMAT(1HK,19H* (H1,H2)=(0.5,1.5),92X,
119H(H1,H2)=(1.5,1.5) *)
840 FORMAT(1HK,19H* (H1,H2)=(0.5,0.0),92X,
119H(H1,H2)=(1.0,0.0) *)
850 FORMAT(1HK,19H* (H1,H2)=(0.5,1.0),92X,
119H(H1,H2)=(1.0,1.0) *)
860 FORMAT(1HK,19H* (H1,H2)=(0.0,0.0),92X,
119H(H1,H2)=(0.5,0.0) *)
870 FORMAT(1HK,19H* (H1,H2)=(0.0,0.5),92X,
119H(H1,H2)=(0.5,0.5) *)
880 FORMAT(1H1,60X,13H1ORDER(H1,H2)/)
890 FORMAT(1H1,33X,35HTHE ORDER INTENSITY WITH SYMMETRY A,
131HCROSS THE 110 LINE BEING FORCED)
895 FORMAT(1H1,60X, 13HMINORD(H1,H2) / )
900 FORMAT(10X,4F8.3 )
1000 FORMAT(1H ,17F7.2)
      DIMENSION DIFUSI(31,61,6), T1H2(31,61,6), T2H2(21,21,6),
      1T1H1(21,21,6), T4(21,21,6)
      REAL IORDER(21,21,6 )
1 READ(5,750) NPTSH1,NPTSH2,NPTSH3
      RD1=NPTSH1-1
      RD2=NPTSH2-1
      RD3=NPTSH3-1
      NP1M1=NPTSH1-1
      NP1P1=NPTSH1+1
      N1=3*NPTSH1-2
      N1I2M1=2*NPTSH1-1
      N1I2=2*NPTSH1

```

```

N1T4M3=4*NPTSH1-3
NP2M1=NPTSH2-1
NP2P1=NPTSH2+1
N2T2M1=2*NPTSH2-1
N2T3M1=3*NPTSH2-1
N2T3M2=3*NPTSH2-2
N2T3M3=3*NPTSH2-3
N2T4M3=4*NPTSH2-3
N2T5M3=5*NPTSH2-3
N2T5M4=5*NPTSH2-4
N2=6*NPTSH2-5
N3=(NPTSH3+1.0)/2.0
IMID=((N1T2M1-NPTSH1)/2.0)+NPTSH1
JMID=((NPTSH2+1.0)/2.0)+N2T3M3
DLTAH1=0.5/RD1
DLTAH2=0.5/RD2
DLTAH3=0.5/RD3
DO 100 K=1,6
  KMK=30+K
2  M=0
  N=0
  DO 210 J=31,61
    KK=J-30
    IF ( J .LT. KMK ) GO TO 85
    KKK=31
    JJ=J-30
    IK=J-30
    I=IK
    IF ( J .GT. 41 ) GO TO 50
    IF ( J .GT. 42-K ) GO TO 14
    IKK=9+K
    GO TO 30
14  IKK=51-J
30  DO 20 I=IK,IKK
20  DIFUSI(I,J,K)=0.0
    CONTINUE
    KIK=20+IK
    IKK1=IKK+1
    KIK1=KIK+1
    DO 40 I=IKK1,KIK
    II=I-10
    M=M+1
    READ(5,770) DIFUSI(I,J,K)
    IF ( DIFUSI(I,J,K) .GE. 0.0 ) GO TO 40
    DIFUSI(I,J,K) =0.0
40  CONTINUE
    DO 48 I=KIK1,KKK
48  DIFUSI(I,J,K)=0.0
    GO TO 300
50  IF ( J .GT. 51 ) GO TO 65

```

```

      IF ( J .GE. 40+K .AND. J .LE. 52-K ) GO TO 55
      KNK=42-IK
      GO TO 60
55  KNK=31
60  IF ( I .GT. KNK ) GO TO 300
      II=I-10
      READ(5,770) DIFUSI(I,J,K)
      I=I+1
      N=N+1
      IF ( DIFUSI(I,J,K) .GE. 0.0 ) GO TO 61
      DIFUSI(I,J,K) =0.0
61  GO TO 60
65  DO 70 I=IK,KNK
70  DIFUSI(I,J,K)=0.0
300 CONTINUE
      GO TO 210
85  DO 250 I=KK,31
250 DIFUSI(I,J,K)=0.0
210 CONTINUE
      NM=N+M
      WRITE(6,17) NM
100 CONTINUE
      DO 103 K=1,N3
      KK=30+K
      DO 103 J=KK,JMID
      JJ=J-30
      DO 103 I=NPTSH1,N1
103 DIFUSI(I,KK,JJ)=DIFUSI(I,J,K)
      DO 105 K=1,N3
      DO 105 J=N2T3M1,N2
      NN=J-N2T3M1+1
      DO 105 I=1,NN
      JREFL1=N2T3M3+I
105 DIFUSI(I,J,K)=DIFUSI(NN+1,JREFL1,K)
      DO 125 K=1,N3
      DO 125 I=1,N1
      DO 125 J=1,N2T3M3
      JREFL2=N2+1-J
125 DIFUSI(I,J,K)=DIFUSI(I,JREFL2,K)
      WRITE(6,700)
      WRITE(6,800)
      DO 128 K=1,N3
      DO 128 J=1,N2
128 WRITE(6,1000)(DIFUSI(I,J,K), I=1,N1 )
      WRITE(6,810)
      DO 145 K=1,N3
      DO 145 J=N2T2M1,N2
      JJ=J+1-N2T2M1
      DO 145 I=1,N1
145 T1H2(I,J,K)=DIFUSI(I,J,K)-DIFUSI(I,JJ,K)
      WRITE(6,710)

```

```

WRITE(6,820)
DO 148 K=1,N3
DO 148 J=N2T2M1,N2
148 WRITE(6,1000) ( T1H2(I,J,K), I=NPTSH1,N1 )
WRITE(6,830)
DO 155 K=1,N3
DO 155 J=NPTSH2,N2T2M1
JJ=J+N2T3M3
JJJ=J+NP2M1
DO 155 I=NPTSH1,N1T2M1
155 T2H2(I,J,K)=T1H2(I,JJ,K) - T1H2(I,JJJ,K)
DO 160 K=1,N3
DO 160 I=NPTSH1,N1T2M1
DO 160 J=1,NP2M1
JJ=N2T2M1+1-J
160 T2H2(I,J,K) = T2H2(I,JJ,K)
DO 165 K=1,N3
DO 165 J=1,N2T2M1
DO 165 I=1,NP1M1
II=N1T2M1+1-I
165 T2H2(I,J,K) = T2H2(II,J,K)
WRITE(6,720)
WRITE(6,840)
DO 168 K=1,N3
DO 168 J=1,N2T2M1
168 WRITE(6,1000) ( T2H2(I,J,K), I=NPTSH1,N1T2M1 )
WRITE(6,850)
DO 170 K=1,N3
DO 170 I=NPTSH1,N1T2M1
II=N1T4M3+1-I
DO 170 J=1,N2T2M1
JJ=N2T3M3+J
170 T1H1(I,J,K) = T1H2(I,JJ,K) - T1H2(II,JJ,K)
DO 172 K=1,N3
DO 172 J=1,NPTSH2
JJ=22-J
DO 172 I=JJ,N1T2M1
II=N1T2-I
172 T1H1(JJ,II,K)=T1H1(I,J,K)
DO 173 K=1,N3
DO 173 J=NPTSH2,N2T2M1
DO 173 I=NPTSH1,N1T2M1
173 T1H1(J,I,K)=T1H1(I,J,K)
DO 175 K=1,N3
DO 175 J=1,N2T2M1
DO 175 I=1,NP1M1
II=N1T2M1+1-I
175 T1H1(I,J,K) = -T1H1(II,J,K)
WRITE(6,730)
WRITE(6,840)
DO 178 K=1,N3
DO 178 J=1,N2T2M1

```

```

178 WRITE(6,1000) ( T1H1(I,J,K), I=NPTSH1,N1T2M1 )
    WRITE(6,850)
    DO 190 K=1,N3
      RK=K-1
      H3=RK*DLTAH3
      DO 190 J=1,N2T2M1
        RJ=J-1
        H2=RJ*DLTAH2
        JJ=N2T3M3+J
        DO 190 I=NPTSH1,N1T2M1
          RI=I-1
          H1=RI*DLTAH1
190  T4(I,J,K) = T1H2(I,J,K) - 0.5*H1*T1H1(I,J,K)-0.5*H3*
      1(-T1H1(I,J,K))+ 0.5*(1.0-2.0*H2)*T2H2(I,J,K)
      DO 195 K=1,N3
        DO 195 J=1,N2T2M1
          DO 195 I=1,NP1M1
            II=N1T2M1+1-I
195  T4(I,J,K) = T4(II,J,K)
      WRITE(6,740)
      WRITE(6,840)
      DO 198 K=1,N3
        DO 198 J=1,N2T2M1
198  WRITE(6,1000) ( T4(I,J,K), I=NPTSH1,N1T2M1 )
      WRITE(6,850)
      DO 200 K=1,N3
        RK=K-1
        H3=RK*DLTAH3
        DO 200 J=1,N2T2M1
          RJ=J-1
          H2=RJ*DLTAH2
          JJ=N2T3M2-1+J
          DO 200 I=NPTSH1,N1T2M1
            RI=I-1
            H1=RI*DLTAH1
200  IORDER(I,J,K) = JIFUSI(I,J,K) -
      1H2*T4(I,J,K)-H1*T4(J,I,K)-H3*T4(I,J,K) -
      20.5*(H1**2)*T2H2(J,I,K)-0.5*(H2**2)*T2H2(I,J,K)-
      30.5*(H3**2)*T2H2(I,J,K) - 0.5*H1*H2*T1H1(I,J,K)-
      40.5*H1*H3*T1H1(I,J,K)-0.5*H2*H3*(-T1H1(I,J,K))
      WRITE(6,880)
      WRITE(6,840)
      DO 1003 K=1,N3
        DO 1003 J=1,N2T2M1
1003 WRITE(6,1000) ( IORDER(I,J,K), I=NPTSH1,N1T2M1 )
      WRITE(6,850)
      DO 1005 K=1,N3
        DO 1005 J=1,NPTSH2
          DO 1005 I=1,NPTSH1
            II=N1T2M1+1-I
1005 IORDER(I,J,K)=IORDER(II,J,K)

```



```

      DO 1400 K=1,N3
      DO 1400 J=1,NPTSH2
      DO 1400 I=1,NPTSH1
1400  WRITE(2,900) IORDER(I,J,K), T4(I,J,K), T2H2(I,J,K),
      1T1H1(I,J,K)
600  CONTINUE
      CALL EXIT
      END

```

C  
C  
C  
C  
C  
C  
C  
C

# PROGRAM COEFFS.

THIS PROGRAM CALCULATES THE FOURIER COEFFICIENTS  
ALPHAS, GAMMAS, DELSQARE AND DELCROSS COEFFS.

```

12  FORMAT(2F5.0, F4.0, 2I3, 15 )
17  FORMAT(20X,15,F8.3 )
18  FORMAT(10X,2I5,F8.3 )
92  FORMAT(1HK,6I5)
300 FORMAT(10X,4F8.3 )
500 FORMAT(3I5)
503 FORMAT(4F10.4 )
880 FORMAT(14I,60X,13HIORDER(H1,H2)/)
1000 FORMAT(14, 17F7.2 )
      DIMENSION X(11), Y(11), Z(11), KL(11), KM(11), KN(11),
1   F(11), FA (11,11), FB (11), FC (11), FD (11),
2F1M(11), FA1M(11,11), FB1M(11), FC1M(11), FD1M(11),
3F2M(11), FA2M(11,11), FB2M(11), FC2M(11), FD2M(11),
4F3M(11), FA3M(11,11), FB3M(11), FC3M(11), FD3M(11)
      DIMENSION SROINT(11,11,11), D2(11,11,11), R2(11,11,11),
1S2(11,11,11), ALPHA(9,9,9), GAMMA(9,9,9),
2DLSQM(9,9,9), DCRLM(9,9,9)

```

```

TWOPI=6.2831853
DELTA=0.0001
READ(5,500) NPTSH1,NPTSH2,NPTSH3
READ(5,500) LMAX,MMAX,NMAX
READ(5,503) SYADJ1,SYADJ2,SYADR2,SYADS2
READ(5,503) DLTAH1,DLTAH2,DLTAH3
NP1P1=NPTSH1+1
NP2P1=NPTSH2+1
NP3P1=NPTSH3+1
N3=(NPTSH3+1)/2
DO 250 K=1,N3
DO 250 J=1,NPTSH2
DO 250 I=1,NPTSH1
250 READ(5,300) SROINT(I,J,K),Q2(I,J,K),R2(I,J,K),
1S2(I,J,K)
DO 510 K=1,N3
II=NP3P1-K
DO 510 J=K,II
JJ=NP2P1-J
DO 510 I=K,II
KK=NP1P1-I
510 SROINT(II,JJ,KK)=SROINT(I,J,K)
DO 520 K=1,N3
JJ=NP2P1-K
DO 520 J=K,JJ
II=NP1P1-K
DO 520 I=K,II
520 SROINT(J,I,K)=SROINT(I,J,K)
DO 530 K=1,N3
KK=NP3P1-K
DO 530 J=K,KK
II=NP1P1-K
DO 530 I=K,II
530 SROINT(I,K,J)=SROINT(I,J,K)
DO 540 I=N3,NPTSH1
KK=NP3P1-I
DO 540 K=KK,I
DO 540 J=K,I
540 SROINT(I,K,J)=SROINT(I,J,K)
DO 550 I=N3,NPTSH1
JJ=NP2P1-I
DO 550 J=JJ,I
KK=NP1P1-I
DO 550 K=KK,I
550 SROINT(K,J,I)=SROINT(I,J,K)
DO 560 K=1,N3
JJ=NP2P1-K
DO 560 J=K,JJ
II=NP1P1-K
DO 560 I=K,II

```

```

560 SROINT(K,J,I)=SROINT(I,J,K)
DO 570 K=N3,NPTSH3
JJ=NP2P1-K
DO 570 J=JJ,K
II=NP1P1-K
DO 570 I=II,K
570 SROINT(I,K,J)=SROINT(I,J,K)
DO 580 K=1,N3
II=NP1P1-K
DO 580 J=1,NPTSH2
JJ=NP2P1-J
DO 580 I=K,II
KK=NP3P1-I
R2(II,JJ,KK)=R2(I,J,K)
580 Q2(II,J,KK)=Q2(I,J,K)
DO 590 K=1,NPTSH3
DO 590 J=1,NPTSH2
DO 590 I=K,NPTSH1
Q2(K,J,I)=Q2(I,J,K)
590 R2(K,J,I)=R2(I,J,K)
DO 595 K=1,N3
KK=NP3P1-K
DO 595 J=1,NPTSH2
DO 595 I=1,NPTSH1
595 S2(I,J,KK)=S2(I,J,K)
DO 360 K=1,NPTSH3
DO 360 J=1,NPTSH2
360 WRITE(6,1000) ( SROINT(I,J,K), I=1,NPTSH1 )
DO 150 L=1,LMAX
KL(L)=L-1
RL=L-1
DO 150 M=1,MMAX
KM(M)=M-1
RM=M-1
DO 150 N=1,NMAX
KN(N)=N-1
RN=N-1
LMN=(KL(L)+KM(M)+KN(N))/2
RRLMN=LMN
RLMN=(RL+RM+RN)*0.50
TSTLMN=ABS(RLMN-RRLMN)
IF(TSTLMN.LE.DELTA) GO TO 400
ALPHA(L,M,N)=0.0
GAMMA(L,M,N)=0.0
DLSOM(L,M,N)=0.0
DCRLM(L,M,N)=0.0
GO TO 140
400 CONTINUE
DO 35 I=1,NPTSH1
BI=I-1
TOPIHL= TWOPI*DLTAH1*BI*RL

```

```

DO 25 J=1,NPTSH2
  BJ=J-1
  TOPIHM= TWOPI*DLTAH2*BJ*RM
  DO 15 K=1,NPTSH3
    BK=K-1
    TOPIHN= TWOPI*DLTAH3*BK*RM
    F(K)=SRJINT(I,J,K)*COS(TOPIHL)*COS(TOPIHM)*COS(TOPIHN)
    F1M(K)=-Q2(I,J,K)*COS(TOPIHL)*SIN(TOPIHM)*COS(TOPIHN)
    F2M(K)=-R2(I,J,K)*COS(TOPIHL)*COS(TOPIHM)*COS(TOPIHN)
    F3M(K)=+S2(I,J,K)*SIN(TOPIHL)*SIN(TOPIHM)*COS(TOPIHN)
15  X(K)= BK*DLTAH3
    CALL SIMP(X,F,FD,NPTSH3)
    FA(I,J)=FD(NPTSH3)
    FB(J)=FA(I,J)
    CALL SIMP(X,F1M,FD1M,NPTSH3)
    FA1M(I,J)=FD1M(NPTSH3)
    FB1M(J)=FA1M(I,J)
    CALL SIMP(X,F2M,FD2M,NPTSH3)
    FA2M(I,J)=FD2M(NPTSH3)
    FB2M(J)=FA2M(I,J)
    CALL SIMP(X,F3M,FD3M,NPTSH3)
    FA3M(I,J)=FD3M(NPTSH3)
    FB3M(J)=FA3M(I,J)
25  Y(J)=BJ*DLTAH2
    CALL SIMP(Y,FB,FD,NPTSH2)
    FC(I)=FD(NPTSH2)
    CALL SIMP(Y,FB1M,FD1M,NPTSH2)
    FC1M(I)=FD1M(NPTSH2)
    CALL SIMP(Y,FB2M,FD2M,NPTSH2)
    FC2M(I)=FD2M(NPTSH2)
    CALL SIMP(Y,FB3M,FD3M,NPTSH2)
    FC3M(I)=FD3M(NPTSH2)
35  Z(I)=BI*DLTAH1
    CALL SIMP(Z,FC,FD,NPTSH1)
    ALPHA(L,M,N)= SYADJ1*FD(NPTSH1)
    CALL SIMP(Z,FC1M,FD1M,NPTSH1)
    GAMMA(L,M,N)= SYADG2*FD1M(NPTSH1)
    CALL SIMP(Z,FC2M,FD2M,NPTSH1)
    DLSQM (L,M,N)= SYADR2*FD2M(NPTSH1)
    CALL SIMP(Z,FC3M,FD3M,NPTSH1)
    DCRLM (L,M,N)= SYADS2*FD3M(NPTSH1)
140 CONTINUE
150 CONTINUE
    CALL SHELL(ALPHA,LMAX,MMAX,NMAX,'ALPHA' )
    CALL SHELL(GAMMA,LMAX,MMAX,NMAX,'GAMMA' )
    CALL SHELL(DLSQM,LMAX,MMAX,NMAX,'DLSQM' )
    CALL SHELL(DCRLM,LMAX,MMAX,NMAX,'DCRLM' )
    WRITE(6,92) NPTSH1,NPTSH2,NPTSH3,LMAX,MMAX,NMAX
    CONTINUE
    CALL EXIT
  END

```

```

SUBROUTINE SIMP(XX,FX,AX,NX)
  DIMENSION XX(21),FX(21),AX(21)
  FNX=NX-1
  DELX=(XX(NX)-XX(1))/FNX
  AX(1)=0.0
  DO 10 IX=2,NX,2
10  AX(IX+1) = AX(IX-1) + (DELX*(FX(IX-1)+4.0*FX(IX)+
    1FX(IX+1)))*0.33333333 )
  RETURN
END

```

```

SUBROUTINE SHELL (COEFF,LMAX,MMAX,NMAX,TITLE )
  THIS SUBROUTINE FINDS THE AVERAGE VALUE OF COEFF IN A
  GIVEN COORDINATION SHELL FOR THE PERMUTATIONS OF THE
  NON-NEGATIVE INTEGER VARIABLES, L,M, AND N.
  INTEGER TITLE
  DIMENSION COEFF( 9, 9, 9),KL(11), KM(11), KN(11)
3002 FORMAT(1H+,2X,4HR**2,7H L M N,11X,5H(LMN),7X,
    15H(NML),7X,5H(NLM),7X,5H(NML),7X,5H(MLN),7X,5H(LNM) )
3003 FORMAT(20X,A5,5(7X,A5) )
3004 FORMAT(6F10.5)
3005 FORMAT(1H0,I6,1X,3I2,4X,6(2X,F10.5) )
  WRITE(6,3003) (TITLE, I=1,6 )
  WRITE(6,3002)
  DELTA=0.0001
  NRSQMX=(LMAX-1)**2+(MMAX-1)**2+(NMAX-1)**2
  DO 900 N=1,NMAX
    KN(N)=N-1
    RN=N-1
    DO 900 M=N,MMAX
      KM(M)=M-1
      RM=M-1
      DO 900 L=M,LMAX
        KL(L)=L-1
        RL=L-1
        NRSQ=KL(L)**2+KM(M)**2+KN(N)**2
        IF(NRSQ .GT. NRSQMX) GO TO 1500
        LMN=(KL(L)+KM(M)+KN(N))/2
        RLMN=LMN
        RRLMN=(RL+RM+RN)*0.5
        TSTLMN=ABS(RLMN-RRLMN)
        IF(TSTLMN .GT. DELTA) GO TO 905
        WRITE(6,3005) NRSQ,KL(L),KM(M),KN(N),COEFF(L,M,N),
          1COEFF(M,N,L),COEFF(N,L,M),COEFF(N,M,L),
          2COEFF(M,L,N),COEFF(L,N,M)
905  CONTINUE
900  CONTINUE
1500 RETURN
END

```

## BIBLIOGRAPHY

1. B. Chakravarti, E. A. Starke, Jr., and B. G. LeFevre, J. of Material Science, 5 (1970) 394.
2. F. W. Ling and E. A. Starke, Jr., Scripta Metallurgica, 5 (1971), 741.
3. J. E. Spruiell and E. E. Stansbury, J. of Physics and Chemistry of Solids, 26 (1965), 811.
4. B. G. LeFevre, H. Grenga and B. Ralph, Philosophical Magazine, 18 (1968), 1127.
5. P. R. Okamoto and G. Thomas, Acta Metallurgica, 19 (1971), 825.
6. F. W. Ling and E. A. Starke, Jr., Acta Metallurgica, 19 (1971), 759.
7. B. G. LeFevre and R. W. Newman, Proceedings of Symposium on Field Ion Microscopy in Physical Metallurgy and Corrosion, Georgia Tech, May, 1968.
8. E. Ruedl, P. Delavignette, S. Amelinckx, Physica Status Solidi, 28 (1968), 305.
9. W. B. Synder and C. R. Brooks, Proceedings of Symposium on Ordered Alloys, Third Bolton Landing Conference, AIME, 1969.
10. P. V. Guthrie and E. E. Stansbury, "X-ray and Metallographic Study of Nickel-Rich Alloys of the Nickel-Molybdenum System II," USAEC Report ORNL-3078, Oak Ridge National Laboratory, Tennessee, July, 1961.
11. P. C. Clapp and S. C. Moss, Physical Reviews, 171 (1968) 764.
12. P. C. Gehlen and J. B. Cohen, Physical Revs., 139 (1965) A844.
13. R. O. Williams, Oak Ridge National Laboratory, ORNL-TM-2866, March, 1970.
14. B. E. Warren and B. L. Averbach, Modern Research Techniques in Physical Metallurgy, ASM (1953) 95.
15. C. J. Sparks and B. Borie, Local Atomic Arrangements Studied by X-ray Diffraction, Gordon and Breach, 1966.
16. B. Borie and C. J. Sparks, Acta Crystallographica, A27 (1971) 198-201.

17. C. J. Sparks, Oak Ridge National Laboratory, Unpublished work.
18. J. E. Eppersom, Ph.D. Dissertation, University of Tennessee, March, 1968.
19. W. Lin and J. E. Spruiell, Acta Metallurgica, 19, (1971), 451.
20. J. Gragg, Ph.D. Thesis, Northwestern University, 1970.
21. B. Borie, Acta Cryst., 14, (1961), 472.
22. D. Harker, Trans. ASM, 1944.
23. R. A. Young, Acta Cryst., A25, (1969), 55.
24. A. H. Compton and S. K. Allison, X-rays in Theory and Experiment, (1935), 780.
25. C. J. Sparks, private communication.
26. J. Gragg, P. Bardhan, and J. B. Cohen, Critical Phenomena in Alloys, Magnets and Superconductors, McGraw Hill, New York, (ed. R. E. Mills, E. Ascher, R. I. Jaffee), p. 309.
27. E. Epremian and D. Harker, J. of Metals, 1, 267 (1949).
28. H. G. Baer, Z. Metallkde, 57(4): 318, (1966).

## VITA

Name: Bhaven Chakravarti

Date of Birth: January 4, 1945

Place of Birth: Patna, Bihar, India

Education:

Indian Institute of Technology Kharagpur, India	Bachelor of Technology in Met. Engineering	May, '67
--	---	----------

Georgia Institute of Technology Atlanta, Georgia	Master of Science in Metallurgy	June, '70
---	------------------------------------	-----------

Married: February 15, 1970

Wife: Nandita Chakravarti

Children: Anita Chakravarti, born June 15, 1973, Atlanta, Georgia

Member: Sigma Xi, American Society for Metals, American Institute of Mining, Metallurgical, and Petroleum Engineers

Publications:

B. Chakravarti, E. A. Starke, B. G. LeFevre, "Order Induced Strengthening in  $\text{Ni}_4\text{Mo}$ ", Journal of Material Science, 5, 1970, p. 394.